

Lawrence Berkeley National Laboratory

Recent Work

Title

SCATTERING OF GAMMA RAYS BY PROTONS BELOW NEUTRAL MESON THRESHOLD

Permalink

<https://escholarship.org/uc/item/2dq9297n>

Author

Higgins, Larry L.

Publication Date

1957-02-14

UNIVERSITY OF
CALIFORNIA

*Radiation
Laboratory*

TWO-WEEK LOAN COPY

*This is a Library Circulating Copy
which may be borrowed for two weeks.
For a personal retention copy, call
Tech. Info. Division, Ext. 5545*

SCATTERING OF GAMMA RAYS BY PROTONS
BELOW NEUTRAL MESON THRESHOLD

BERKELEY, CALIFORNIA

DISCLAIMER

This document was prepared as an account of work sponsored by the United States Government. While this document is believed to contain correct information, neither the United States Government nor any agency thereof, nor the Regents of the University of California, nor any of their employees, makes any warranty, express or implied, or assumes any legal responsibility for the accuracy, completeness, or usefulness of any information, apparatus, product, or process disclosed, or represents that its use would not infringe privately owned rights. Reference herein to any specific commercial product, process, or service by its trade name, trademark, manufacturer, or otherwise, does not necessarily constitute or imply its endorsement, recommendation, or favoring by the United States Government or any agency thereof, or the Regents of the University of California. The views and opinions of authors expressed herein do not necessarily state or reflect those of the United States Government or any agency thereof or the Regents of the University of California.

UCRL-3688
Physics and Mathematics

UNIVERSITY OF CALIFORNIA

Radiation Laboratory
Berkeley, California

Contract No. W-7405-eng-48

SCATTERING OF GAMMA RAYS BY PROTONS
BELOW NEUTRAL MESON THRESHOLD

Larry L. Higgins

(Thesis)

February 14, 1957

Printed for the U. S. Atomic Energy Commission

SCATTERING OF GAMMA RAYS BY PROTONS
BELOW NEUTRAL MESON THRESHOLD

Contents

Abstract	3
I. Introduction.	4
Thomson scattering	6
The Klein-Nishina formula.	7
Anomalous magnetic moment scattering	8
Mesonic polarization scattering	9
II. The Experiment	
A. General Discussion	13
B. The Experimental Layout	17
C. Gamma-Ray Source	21
D. Hydrogen Target	23
E. Detector	25
F. Electronics	27
G. Photographic Method	36
H. Experimental Procedure.	37
I. Experimental Results.	39
III. Analysis of the Data	
A. Film Reading	41
B. Background	42
C. Bremsstrahlung Spectra	47
D. Gamma-Ray Detector Efficiency	49
E. Calculation of the Cross Section	68
IV. Results	
A. Discussion of the Results	74
B. Comparison with Theory	76
C. Comparison with Other Experiments	84
D. Summary	86
Acknowledgments	87
Bibliography	88

SCATTERING OF GAMMA RAYS BY PROTONS
BELOW NEUTRAL MESON THRESHOLD

Larry L. Higgins

Radiation Laboratory
University of California
Berkeley, California

February 14, 1957

ABSTRACT

The differential cross section for the elastic scattering of gamma rays by protons at 90° has been measured in the bremsstrahlung beam at the Berkeley synchrotron. The measurements were carried out below the threshold energy for neutral meson production, in the energy region from 40 to 132 Mev. The gamma-rays scattered from a liquid hydrogen target are detected by a converter telescope and recorded photographically. The recoil proton is not detected. The energy dependence of the cross section is obtained by the photon-difference method. The cross section is found to be an increasing function of photon energy, and indicates that the scattering due to the anomalous magnetic moment of the proton and its interference with the mesonic polarization scattering are necessary additions to the proton Klein-Nishina cross section. The absolute differential cross section at 90° in the low-energy region of this experiment was found to be approximately 30% higher than the Thomson cross section.

SCATTERING OF GAMMA RAYS BY PROTONS BELOW NEUTRAL MESON THRESHOLD

I. INTRODUCTION

Gamma-ray scattering by protons is of fundamental importance because it involves the interaction of two elementary particles: the quantum of the electromagnetic field and the charged building block of nuclear matter, the proton. Many aspects of this scattering phenomenon are very similar to another fundamental process already well known to physicists: the Compton effect. A notable addition, however, in the scattering of radiation by protons, is the effect of the anomalous magnetic moment of the proton and of the structure provided by the cloud of virtual charged mesons about the proton arising from its strong interaction with the meson field. In view of the effects of mesonic origin, as photon energies approach the threshold energy for the photoproduction of mesons in hydrogen, deviations from the scattering expected from a proton without structure should become apparent.

The corpuscular nature of the scattering process and its treatment in terms of relativistic dynamics, which were of such pointed interest in the Compton electron effect, are taken for granted in the proton scattering. The Compton wave-length shift for proton scattering is

$$\Delta \lambda = 2 \pi \left(\frac{\hbar}{Mc} \right) (1 - \cos \theta),$$

where θ is the scattering angle and $\frac{\hbar}{Mc}$ is the nucleon Compton wave length, which is the small distance

$$\frac{\hbar}{Mc} = 2.10 \times 10^{-14} \text{ cm.}$$

An example of an elastic scattering event for an incident-photon energy equal to the threshold energy for the photoproduction of neutral pi mesons in hydrogen is illustrated in Fig. 1 in order to show the typical

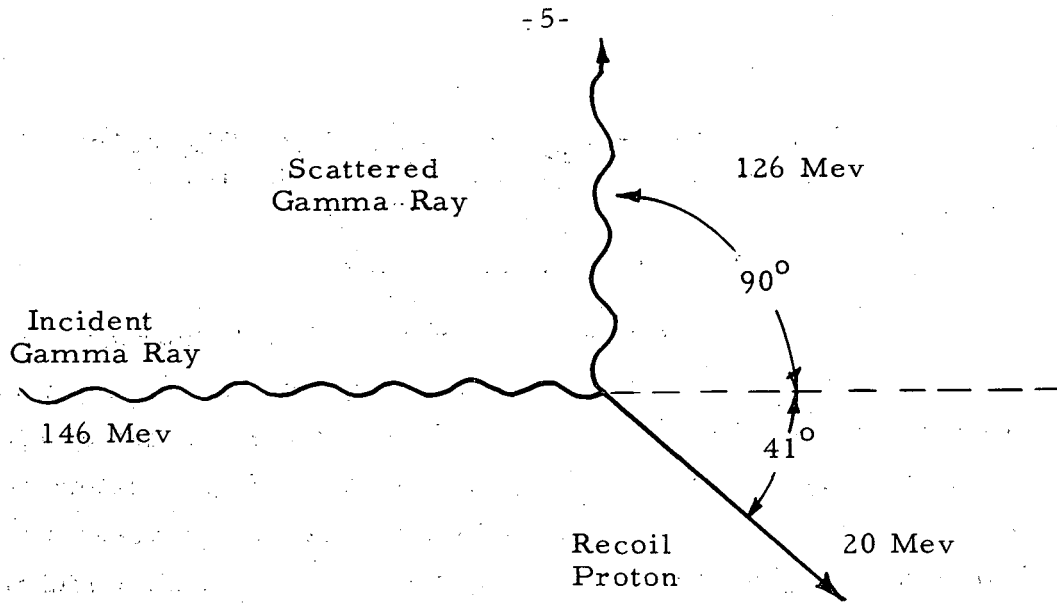


Fig. 1. Example of a scattering event.

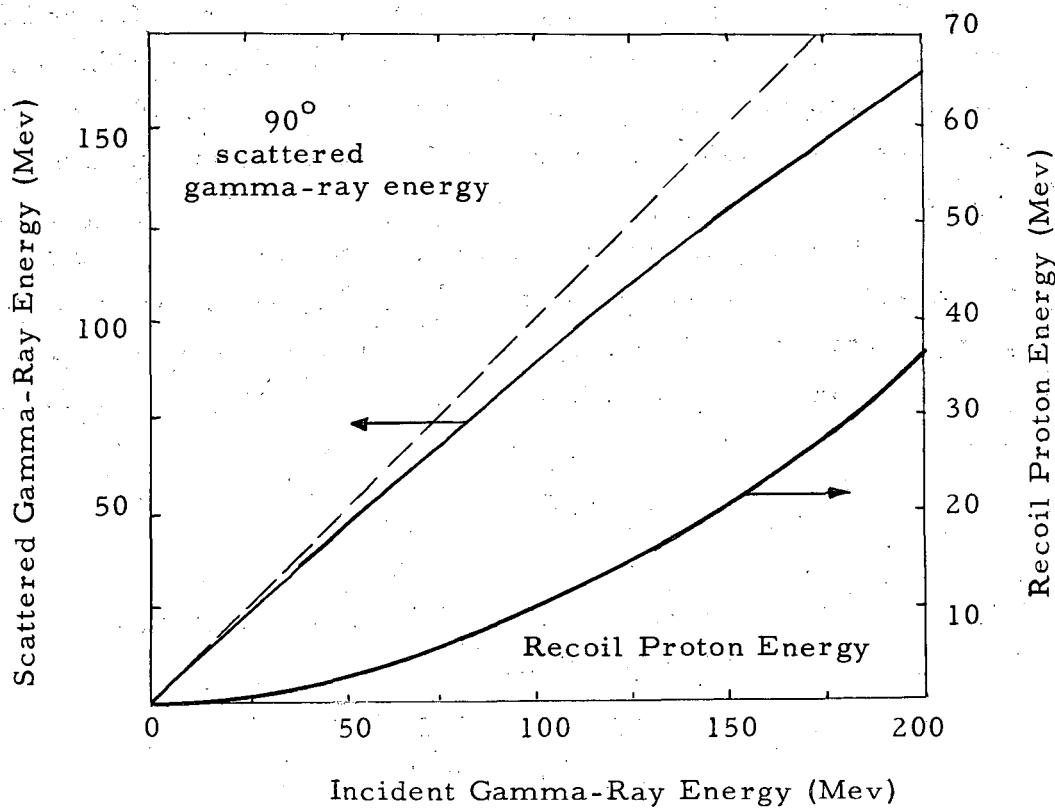


Fig. 2. Gamma-ray and proton energies for 90° scattering angle.

energies involved. Figure 2 shows the scattered gamma-ray energy, k' , and the recoil-proton energy, $k-k'$, for 90° scattering angle versus incident photon energy k as obtained from the Compton relation

$$k' = \frac{k}{1 + \alpha(1 - \cos \theta)}$$

where $\alpha = k/Mc^2$. In the low-energy limit, the incident and scattered rays have the same energy.

The salient features in the theory of the scattering cross section are briefly, as follows.

Thomson Scattering. For quanta much less energetic than the rest-mass energy of the proton, Mc^2 or 938 Mev, the scattering cross section can be calculated classically, and is given by the Thomson formula. The incident radiation subjects the scatterer to forced vibrations, and -- because of the acceleration of the associated charge -- radiation is emitted or scattered from the proton. The total cross section obtained from the classical radiation formula is the familiar Thomson total cross section, with the mass of the proton replacing the electron mass:

$$\sigma_T = \frac{8}{3} \pi \left(\frac{e^2}{Mc^2} \right)^2$$

The Thomson scattering is independent of the photon energy. Since the scattering varies inversely as the square of the mass of the target particle, the cross section is smaller than that for electrons by a factor of $(1837)^2$, or about three million, and puts the proton Thomson total cross section at the small value of

$$1.98 \times 10^{-31} \text{ cm}^2$$

The angular distribution for unpolarized radiation is

$$\frac{d\sigma}{d\Omega} = \frac{1}{2} \left(\frac{e^2}{Mc^2} \right)^2 (1 + \cos^2 \theta),$$

and at 90° scattering angle the differential cross section amounts to

$$\frac{1}{2} \left(\frac{e^2}{Mc^2} \right)^2 = 1.18 \times 10^{-32} \text{ cm}^2/\text{steradian}.$$

The Klein-Nishina Formula. The scattering of electromagnetic radiation from a point particle of charge e , mass M , spin $1/2$, and magnetic moment $\left(\frac{e\hbar}{2Mc}\right)$ is treated according to the Dirac theory when the photon energies are not small compared with the rest-mass energy of the scatterer. For unpolarized radiation the differential cross section obtained is the famous Klein-Nishina formula,

$$\frac{d\sigma}{d\Omega} = \frac{1}{2} \left(\frac{e^2}{Mc^2} \right)^2 \left(\frac{a'}{a} \right)^2 \left[(1 + \cos^2 \theta) + aa' (1 - \cos \theta)^2 \right]$$

where the incident and scattered photon energies are measured in units of Mc^2 : $k = aMc^2$, $k' = a'Mc^2$. The factors that appear in the Klein-Nishina formula are, from left to right, (a) the basic unit of cross section for elastic photon scattering, (b) a factor which accounts for the transformation of solid angle from the frame of the recoiling scatterer (proton) to the laboratory frame, (c) the angular distribution of Thomson scattering, and (d) the specific Klein-Nishina term, that accounts for the effect of the interaction of the incident quanta with the intrinsic magnetic moment associated with the spin angular momentum of the particle. For the proton, the Dirac-moment term is quite small (2%) for photon energies below 140 Mev; however, at this energy the recoil factor amounts to a 20% reduction below the Thomson cross section.

Anomalous Magnetic Moment Scattering. The magnetic moment of the proton is not one nuclear magneton -- as would be expected if it were a pure Dirac particle, which is not in interaction with other particle fields -- but the relatively large value,

$$2.7896 \left(\frac{e\hbar}{2Mc} \right)$$

The anomalous part of the proton magnetic moment (1.7896 nm) should make an additional contribution to the scattering of gamma rays. The scattering associated with the magnetic moment due to the coupling with electric and magnetic fields of the photon arises from the consequent acceleration of the proton as follows: (a) translational vibration of the magnetic moment under the action of the electric field on the charge, (b) rotational vibration of the magnetic moment under the action of the magnetic field on the magnetic moment, (c) translational vibration of the charge due to the gradient of the magnetic field acting on the magnetic moment. These contributions go to zero as the wave length becomes long compared with the dimensions of the magnetic moment. Powell¹ and, more recently, Low,² Gell-Mann,³ and Klein,⁴ have treated the scattering from a point anomalous magnetic moment, and their result is valid for photon energies low enough so that the magnetic moment remains equal to the static value. The differential cross section for unpolarized rays is

$$\frac{d\sigma}{d\Omega} = \frac{1}{2} \left(\frac{e^2}{Mc^2} \right)^2 \left(\frac{a'}{a} \right)^2 \left[(1 + \cos^2\theta) + a a' (1 - \cos\theta)^2 + a a' f(\theta) \right],$$

where

$$f(\theta) = A + B \cos\theta + C \cos^2\theta,$$

and

$$A = 2\lambda + \frac{9}{2}\lambda^2 + 3\lambda^3 + \frac{3}{4}\lambda^4 = 42.88,$$

$$B = -4\lambda - 5\lambda^2 - 2\lambda^3 = -34.63,$$

$$C = 2\lambda + \frac{1}{2}\lambda^2 - \lambda^3 - \frac{1}{4}\lambda^4 = -3.12,$$

and

$$\lambda = 1.7896.$$

This expression is exactly the same as the Klein-Nishina formula except for the last term in the square bracket, which is attributable to the effect of the anomalous magnetic moment. This cross section, called the Powell cross section, is illustrated in Fig. 3 and 4 along with the Klein-Nishina and Thomson cross sections. At 90° scattering angle this term is 43 times as large as the intrinsic moment term for 146-Mev photons, and leads to an 86% increase over the Klein-Nishina cross section. The magnetic moment scattering favors the backward hemisphere.

Mesonic Polarization Scattering. As a consequence of the interaction between the proton and the pion field there is a cloud of preferentially positive mesons surrounding the proton which is not rigidly attached and may be polarized, both electrically and magnetically, by incident photons. This coupling of the photon to the proton provides an additional means of scattering which contributes to, and interferes with, the scattering by the static electric charge and the magnetic moment of the proton.

The order of magnitude of this effect is now estimated. The scattering cross section of low-energy photons by free positive mesons is presumably given by the Thomson expression,

$$\frac{8}{3} \pi \left(\frac{e^2}{\mu c^2} \right)^2, \quad \mu c^2 = 141 \text{ Mev},$$

which is $(M/\mu)^2$ or 44 times as large as the corresponding proton

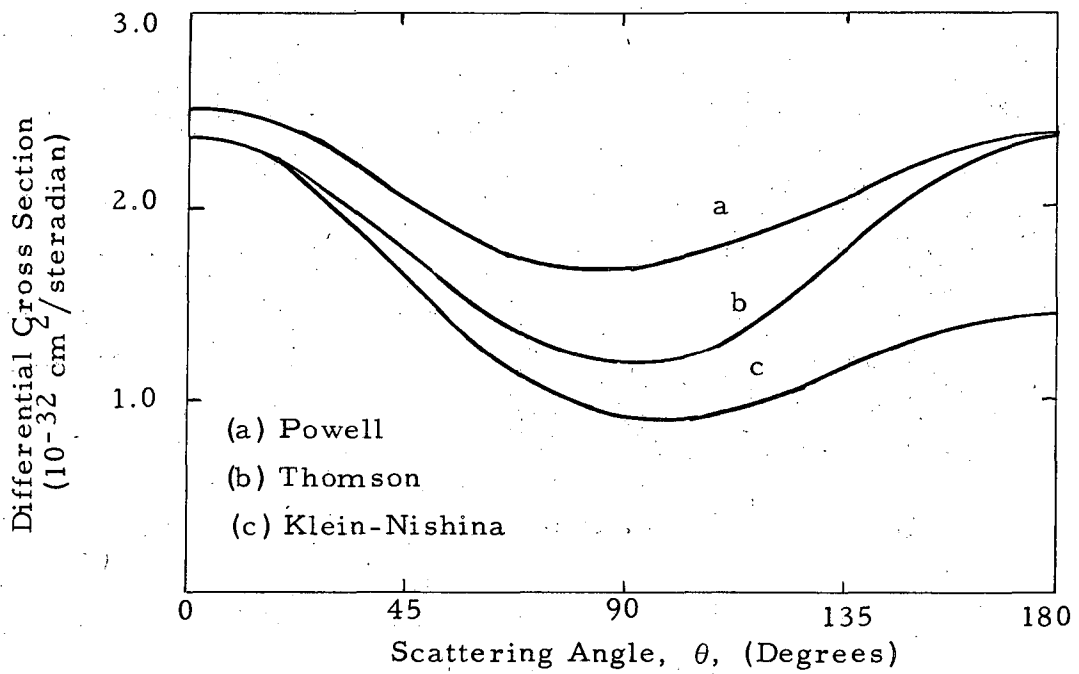


Fig. 3. $\frac{d\sigma}{d\Omega}$ for 146-Mev gamma rays.

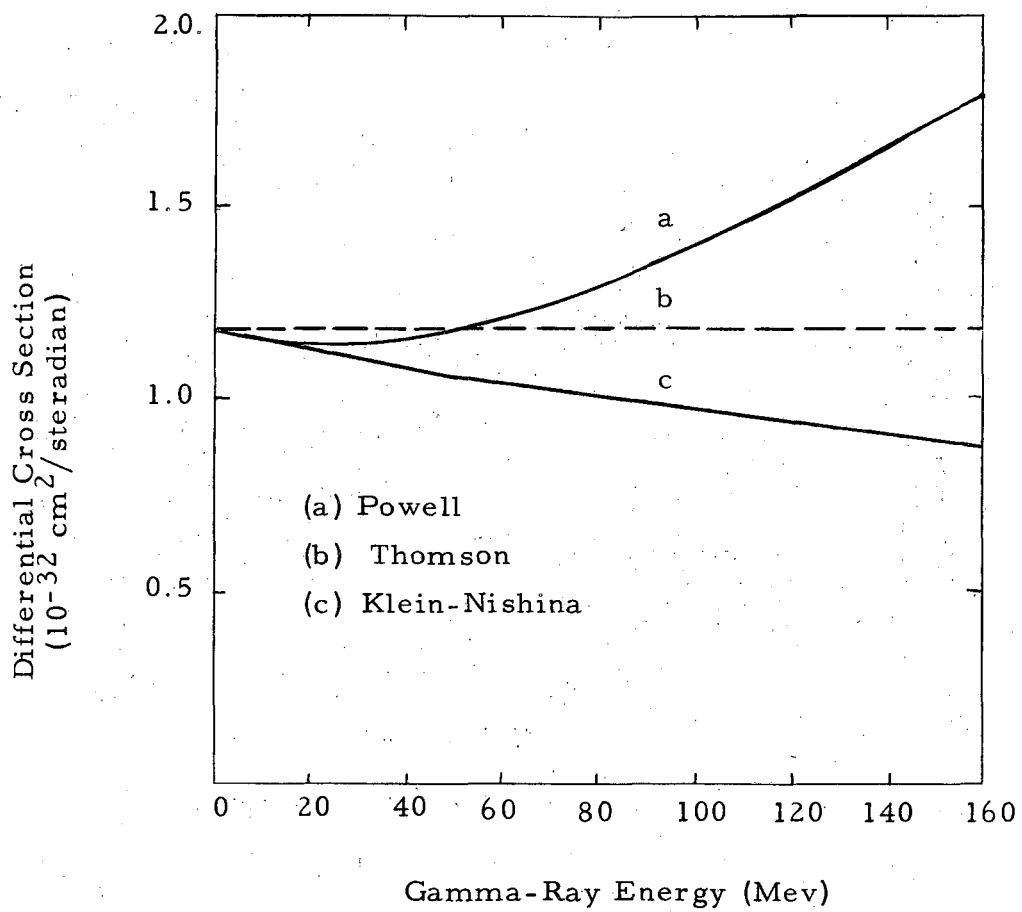


Fig. 4. $\frac{d\sigma}{d\Omega}$ for 90° scattering angle.

value; hence, even the infrequent presence of mesons about the proton should be observable in its effect on the elastic scattering by protons. Let us suppose the fraction of time that charged mesons are present is z . Further, if it is assumed that the period of the incident radiation is long compared with the time that mesons are allowed to be present by the uncertainty principle, then the incident radiation causes an average displacement of the meson cloud, and a dipole is induced which oscillates with the frequency of the incident photons. An oscillating dipole emits radiation which varies as the fourth power of the frequency (Rayleigh scattering), and in this approximation the mesonic-polarization scattering becomes

$$z^2 \left(\frac{M}{\mu} \right)^2 \left(\frac{k}{\mu c^2} \right)^4 \sigma_{\text{proton}}$$

If mesons are present 15% of the time, then, according to this expression, at the threshold for meson production a contribution comparable to the proton Thomson scattering is obtained.

If the mesonic contribution is assumed to be properly described by an electric and magnetic polarizability of the proton's meson cloud, then the scattering due to the Thomson and spin-independent polarization parts, but not the magnetic-moment scattering, is given by the Rayleigh-Thomson scattering formula,^{4, 5}

$$\frac{d\sigma}{d\Omega} = \frac{1}{2} \left(\frac{e^2}{Mc^2} \right)^2 \left(\frac{a'}{a} \right)^2 \left[\{ (1 - A_E a^2)^2 + A_M^2 a^4 \} (1 + \cos^2 \theta) - 4A_M a^2 (1 - A_E a^2) \cos \theta \right],$$

where $A_E a^2$ and $A_M a^2$ are the electric and magnetic dipole amplitudes of the induced spin-independent polarization. The polarization amplitudes in this simple model may be obtained from the experimentally known cross sections for photopion production from protons. It is known that the production of pions arises from the absorption of electric-dipole (π^+) and magnetic-dipole (π^+ and π^0) radiation, hence scattering is to be expected from these same absorption modes.

In the above cross section the electric-polarization scattering interferes at all angles with the proton Thomson scattering, and the magnetic-polarization scattering interferes destructively with it in the forward direction and constructively in the backward direction.

The Rayleigh scattering formula accounts only for the spin-independent polarization of the proton; however, as the polarization scattering is of a mesonic origin and the photoproduction of mesons proceeds through a spin-dependent interaction, one would expect a contribution to the polarization scattering which depends on the spin of the proton.

The final cross section for the scattering must include the contributions from the proton charge, the magnetic moment (both the intrinsic and anomalous parts), and the electric and magnetic polarization of the meson cloud (both the spin-dependent and spin-independent parts), and the interference between these various contributions. The details of the resultant scattering cross section are taken up in Section IV-B.

Several theoretical approaches to the scattering of photons by protons are available in the literature.⁶⁻¹⁰ In particular, it has recently been shown by Gell-Mann, Goldberger, and Thirring¹¹ that, on the basis of very general wave mechanical arguments, certain relations concerning the elastic-scattering cross section may be obtained from a knowledge of the total gamma-ray absorption cross section for protons. By means of these dispersion relations and a knowledge of the total photopion cross section at all energies, it is possible to show that the elastic forward scattering near meson threshold should be small compared with the Thomson value. Furthermore, dispersion relations give information on the sign and magnitude of the spin-independence polarization amplitudes A_E and A_M , and the spin-dependent polarization amplitudes.

The finite size of the proton influences the scattering through the interference between different portions of the charge cloud and becomes important as the wave length of the gamma ray approaches the dimensions of the proton. In exact analogy to the X-ray scattering by

an atom, the interference is accounted for by a form factor, f , which becomes of increasing importance at high energy and large scattering angles. The scattering corrected for finite size is then $f^2 \frac{d\sigma}{d\Omega}$. At the energies of this experiment the form factor is nearly equal to one.

Drelbrück scattering, or the scattering of photons by a fixed Coulomb field due to virtual pair production and annihilation, contributes to the elastic scattering of gamma rays by protons; however, the cross section is very small (10^{-34} cm^2), and is strongly peaked in the forward direction. It is of negligible importance in this experiment.

II. THE EXPERIMENT

A. General Discussion

The differential cross section at 90° for elastic gamma-ray scattering from protons in a vacuum liquid hydrogen target has been measured, by use of the bremsstrahlung beam at the Berkeley synchrotron. Information on the scattering cross section was obtained for gamma-ray energies ranging from 40 to 130 Mev. The process was measured by counting the high-energy gamma rays, scattered at $90^\circ \pm 16^\circ$ to the beam line. The energy dependence of the cross section was found by counting at three different synchrotron energies -- 95, 113, and 132 Mev -- and then, by means of the photon difference method, the yields were analyzed to get the cross sections. The gamma rays are detected with a conventional converter telescope which subtends a rather large solid angle, and does not respond to gamma rays of energy less than 35 Mev. Because of the low cross section being observed (10^{-32} cm²/steradian) and the high background conditions experienced, the detector consisted of four plastic scintillation counters and a Cerenkov counter, all in fivefold coincidence. Further, to insure the reliability of the data collection, all events that appeared to be high-energy gamma rays were recorded photographically and then analyzed visually.

The method of detecting the occurrence of a Compton proton-scattering event by counting only the scattered high-energy gamma ray, without a coincidence with the recoil proton, has been utilized, since the phenomenon of a high-energy photon produced at large angles in the lowest-Z material, hydrogen, is extremely rare, if not dynamically impossible for some processes. The main absorption modes of high-energy X-rays strongly favor the emission of the high-energy resultant particles at small angles to the beam line. The photons scattered from protons retain most of their initial energy, even to the backwardmost scattering angles, since the proton is a massive scatterer compared with the energy of the quanta considered in this experiment

(100 Mev versus 938 Mev). Thus, gamma-ray scattering from protons is the outstanding process to generate high-energy quanta at large angles.

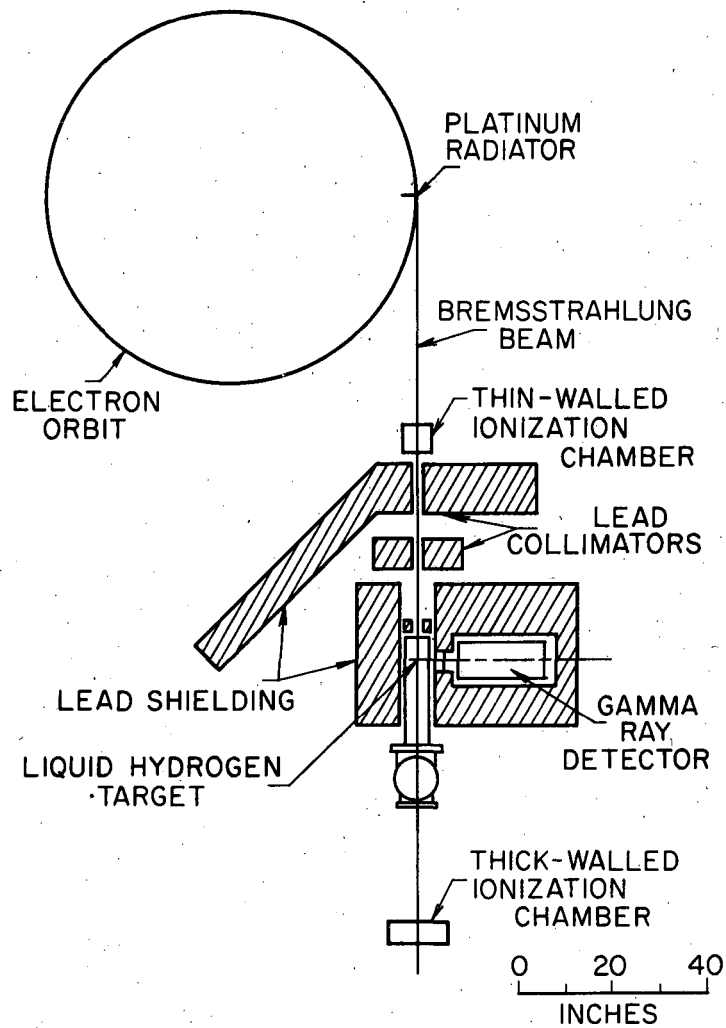
The above remarks are valid only for peak bremsstrahlung energies less than the threshold energy for the photoproduction of neutral mesons in hydrogen. Above this threshold, 146 Mev, energetic (70-Mev) gamma rays due to the decay of π^0 mesons are emitted in all directions, and are confused with the gamma rays elastically scattered from protons. Since there are two decay gamma rays for each neutral meson, and the cross section for π^0 production rises rapidly with photon energy to a value very much larger than the elastic-scattering cross section, it is essential that the synchrotron be operated at energies below 146 Mev lest the Compton proton events be swamped by the gamma rays from neutral mesons.

It would be most desirable to detect a gamma-ray scattering event by requiring a coincidence between the scattered gamma ray and the recoil proton. Since it is a two-body process, a measurement of the energy and angle of the recoil proton in coincidence with the scattered gamma ray would be a conclusive identification of such an event, and further, it would not be necessary to employ the photon-difference method. This was not done in this experiment, since a target thick enough for a workable counting rate is too thick to allow the recoil proton to escape from the target. A typical recoil proton travels less than one inch in liquid hydrogen.

The electron analog process of this experiment, the Compton electron effect, occurs at a rate three million times as great as that of the proton-scattering events. Though the scattering from electrons is more frequent, the photons that are scattered at 90° are limited to a maximum energy equal to the rest-mass energy of the electron by the requirements of the conservation of relativistic momentum and energy. Inasmuch as the threshold energy of detection of the converter telescope is well above 0.51 Mev, these low-energy quanta present no problem.

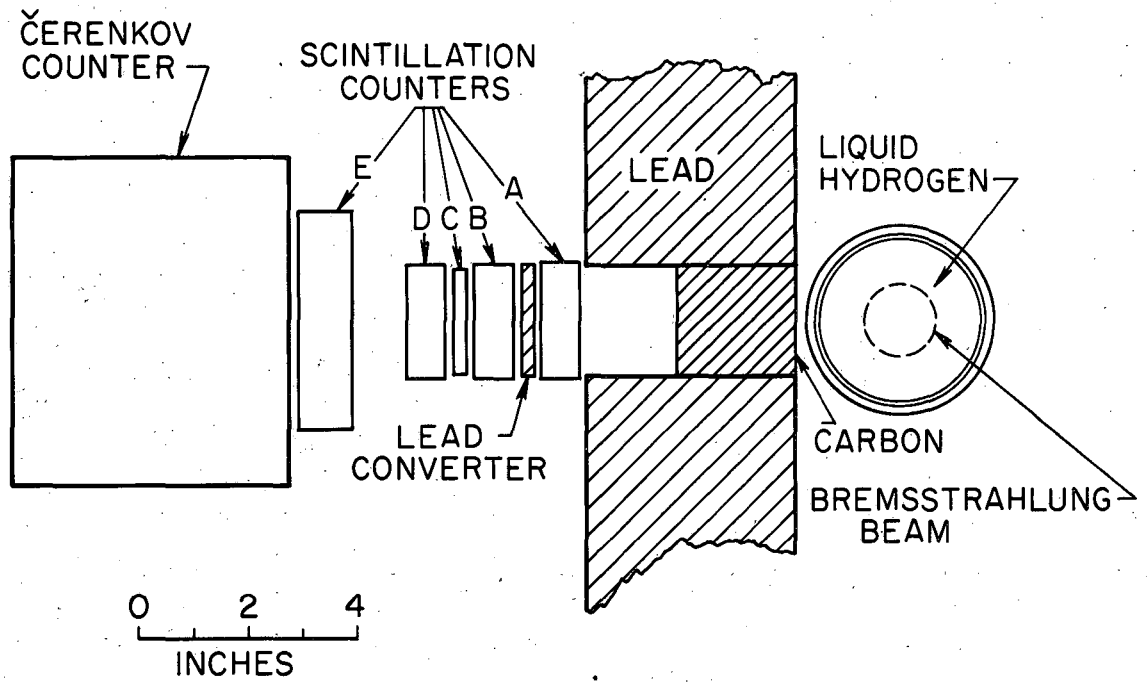
B. The Experimental Layout

Diagrams of the experimental arrangement are shown in Figs. 5, 6, 7. The synchrotron X-ray beam passes through a 3/4-inch-diameter lead collimator, 55.5 inches from the platinum bremsstrahlung target, then through a secondary lead collimator which is slightly larger than the beam defined by the primary collimator and is intended to clean up the "spray" due to the primary collimation. It is estimated that only 7% of the total X-ray output from the synchrotron, set at 132 Mev, passes through the 3/4-inch collimator into the experimental area. The rest of the beam (93%) is lost into the lead wall near the collimator hole, and produces an intense neutron background. At 96 inches from the X-ray source is located the effective volume of the liquid hydrogen target, where the beam diameter is 1.30 inches. Still further collimation was found to be necessary just before the hydrogen target, to insure that any remaining fringe of the beam not hit the walls of the hydrogen target. This collimation consisted merely of a 2-inch-thick lead brick with a hole in it that amply cleared the beam but cast a shadow enveloping the walls of the liquid hydrogen target. After the beam passes through the hydrogen, it strikes a thick-walled ionization chamber (Cornell chamber) with which the beam is monitored. The beam is also monitored by a thin-walled ionization chamber (Nunan chamber) located before the primary lead collimator. The hydrogen target is viewed at 90° by the gamma-ray detector, which is heavily shielded with lead.



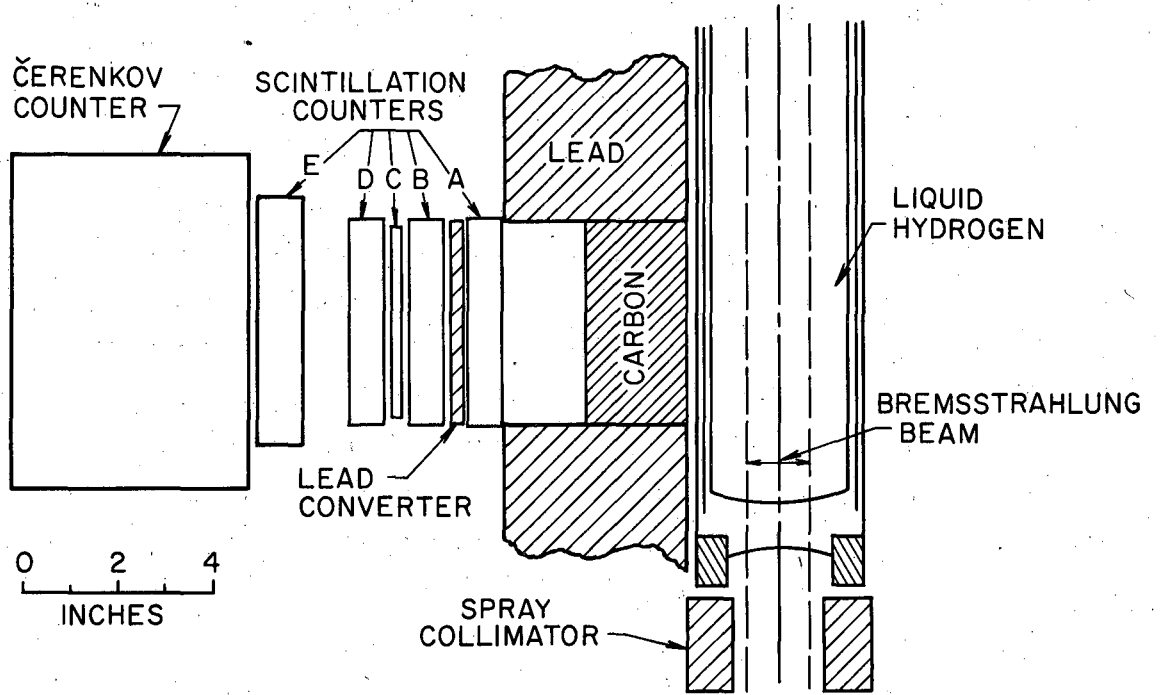
MU-13139

Fig. 5. Experimental layout at the synchrotron.



MU-13140

Fig. 6. Experimental arrangement (viewed parallel to the beam axis).



MU-13141

Fig. 7. Experimental arrangement (plan view).

C. Gamma-Ray Source

The beam of gamma rays to be scattered from protons originates in the synchrotron, where the electrons that have been accelerated to high energy are allowed to strike a 0.020-inch thick platinum target, from which in turn is emitted a bremsstrahlung beam, with its characteristic continuous distribution of X-ray energies up to a maximum energy equal to the peak energy of the electrons in the synchrotron. It is required to obtain bremsstrahlen of energies less than 146 Mev, that is, below the threshold energy for neutral-meson photoproduction in hydrogen. The Berkeley synchrotron may be lowered from its usual energy of 342 Mev by either lowering the peak magnetic field or shortening the rf acceleration period, or both. The energy of the circulating electrons in the synchronous orbit varies sinusoidally with time and is proportional to the peak magnetic field, and hence to the voltage on the magnet capacitor bank. This relation is expressed in the formula

$$k_m = 342 \left(\frac{V}{14.9} \right) \sin \left[90^\circ \left(\frac{7790 - T}{7790} \right) \right],$$

where k_m is the synchrotron energy in Mev (the maximum bremsstrahlung energy), V is the capacitor high voltage in kv, and T is the time in microseconds before the peak magnetic field; 7790 microseconds is 1/4 of the natural period of the magnet-capacitor resonant circuit. At 342 Mev, the capacitor bank voltage is 14.9 kv.

The energies below neutral meson threshold were obtained by changing both V and T . With V equal to 7.6 kV, and T ranging from 4760 to 3100 microseconds, spread-out beams of 100 microseconds were used and easily obtained.

The calculated machine energies were checked, experimentally, by investigating the high-energy end of the bremsstrahlung spectrum with a high-resolution pair spectrometer. The measured values were found to be 6% lower than expected from calculation. In an experiment preceding this one, Anderson and Kenny¹² found close agreement between the measured and calculated values.

Prior to this experiment, disassembly of the synchrotron magnet was necessary to replace a broken quartz, and it is believed that the observed 6% discrepancy is due to slightly different conditions in reassembly. The shift in machine energy is supported, also, by the fact that the counting rate, due to neutral meson-decay gammas, did not begin its steep rise, as the bremsstrahlung energy was increased above threshold, as quickly as was observed in a previous experiment. Coincidentally, 342 Mev/1.06 is 322 Mev, the maximum energy quoted for the Berkeley synchrotron in 1950.¹³

The error in k_m may be calculated from the uncertainty in estimating the time T ($\pm 50 \mu\text{sec}$), the beam spill-out time ($100 \mu\text{sec}$), the random fluctuation in the magnet voltage V , which was monitored on a recording and found to be ± 50 volts, and the uncertainty in the pair-spectrometer measurements ($\pm 3\%$). The final relative error in k_m is ± 2 Mev, and an absolute error ± 4 Mev.

The bremsstrahlung beam is monitored by a thin-walled ionization chamber located before the beam collimators and a thick-walled ionization chamber located some distance behind the liquid hydrogen target. The purpose of these chambers was to make a relative measure of the beam intensity, and the actual sensitivity of the chambers is not used in the calculation of the cross section because of the way in which the gamma-ray detector is calibrated. This is discussed in a later section.

A table of the average beam intensity realized throughout the experiment with the 3/4-inch collimator is given below. The sensitivity of the thick-walled ionization chamber is taken to be 3.30×10^{12} Mev/ $\mu\text{coulomb}$.

k_m Mev	Equivalent Quanta/sec	Cornell chamber $\mu\text{coulomb/hr}$	Background meter mr/hr
95	2.1×10^7	2.2	80
113	3.2×10^7	3.9	125
132	4.0×10^7	5.8	180

D. Hydrogen Target

Several considerations indicate the necessity for a vacuum liquid hydrogen target for this experiment. A polyethylene-carbon subtraction would lead to serious difficulties at the low counting rates expected. The yield of a high-pressure gas target would be too low, and the target-to-background ratio would not be favorable. A styro-foam liquid hydrogen target, though simple, would not be suitable for a long experiment because of its high consumption rate. A large and accessible volume of hydrogen was provided by the target of this experiment, a drawing of which is shown in Fig. 8. The long probe design allows unrestricted shielding and counter arrangement. The large size of the target was desirable because of its higher counting rate and because the effective portion of the target, viewed by the counter and defined by the beam diameter, is immersed in a liquid hydrogen medium, so that wall scattering effects are minimized. This design led to a (full-target/empty-target) ratio of seven.

The entrance foils are 0.001- and 0.002-inch-thick stainless steel. The hydrogen column is 2.88 inches in diameter, which clears the beam diameter by 0.79 inch (as the beam diameter is 1.30 inches). The total volume of hydrogen of the column and reservoir is 8.3 liters, and the liquid nitrogen reservoir holds 11 liters. The hydrogen column is contained in a 0.020-inch brass pipe which is surrounded by and separated from a 0.020-inch copper pipe, connected thermally to the liquid nitrogen reservoir. This system is then surrounded by a 0.0625-inch aluminum vacuum jacket. These three cylinders are held accurately coaxial by small teflon spacers. Thinner walls would have been desirable, as they give rise to background counts due to bremsstrahlen from electrons scattered at wide angles and absorb about 4% of the real counts. The hydrogen consumption, after steady conditions have been reached, is roughly 1 liter per 8 hours. Twenty-five liters of hydrogen were consumed, however, before stable conditions were reached. The effective length of the liquid hydrogen viewed by the counter is 12.0 cm. With the density of liquid hydrogen at $0.071/\text{cm}^3$,

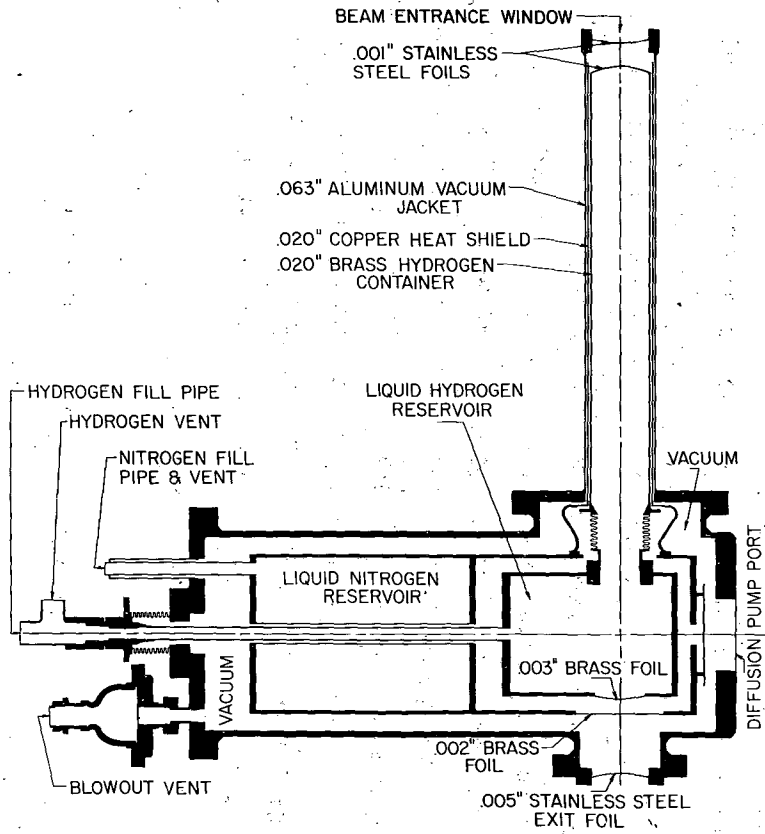


Fig. 8. Diagram of the liquid hydrogen target.

the target thickness is 0.855 g/cm^2 , or

$$nL = 5.13 \times 10^{23} \text{ protons/cm}^2.$$

E. Detector

The detector is intended to count, with relatively high efficiency, gamma rays of energy greater than about 40 Mev. The unit is a conventional gamma-ray converter telescope consisting of a 0.25-inch lead radiator, followed by five counters in (photographic) coincidence, four of which are plastic scintillation counters and one a lucite Cerenkov counter. The B, D, and Cerenkov counters are in electronic triple coincidence. A plastic scintillation anticoincidence counter intended to reject coincidences due to charged particles (electrons) is situated in front of the telescope. The details of the detector geometry are shown in Figs. 6 and 7, and the specifications of the individual counters are listed in Table I. The high coincidence multiplicity of this telescope was found to be necessary, experimentally, to identify conclusively the counts due to gamma rays. One is compelled to use this stringent means of identification because of the low cross section being observed, the high singles counting rates typical of the synchrotron experimental area, and the detection of only the scattered photon (not in coincidence with the recoil proton). The detector is guarded by a 2.25-inch-thick carbon absorber in front of the anticoincidence counter, planned to stop low-energy electrons from the target. On traversing the block, a fast electron suffers an 18-Mev ionization loss. The radiation loss by fast electrons in the carbon is discussed in Section III-D. The efficiency of the anticoincidence counter has been determined, from pulse-height measurements on film, to be $98.0 \pm 0.8\%$ efficient. The 2% inefficiency is not troublesome, because the ratio of anticoincidence counts to real counts is less than 1/3. The effective solid angle of the detector is about 0.1 steradian, and the efficiency for 100-Mev gamma rays is 24%. The energy dependence of the counter efficiency is treated in Section III-C.

Table I "Specifications of Counters"

Counter	A	B	C	D	E	Cer.
Purpose	Anti	Coinc.	co.	co.	co.	co.
Phototube	1P21	1P21	1P21	1P21	1P21	6810(two)
Material	Scint.	Scint.	Scint.	Scint.	Scint.	Lucite
Thickness (in.)	0.75	0.75	0.25	0.75	1.00	5.00
Width (in.)	4.25	4.25	4.00	4.25	5.00	7.00
Height (in.)	2.25	2.13	2.00	2.13	4.00	6.00
Half-width uniformity (%)	15	15	15	15	10	30

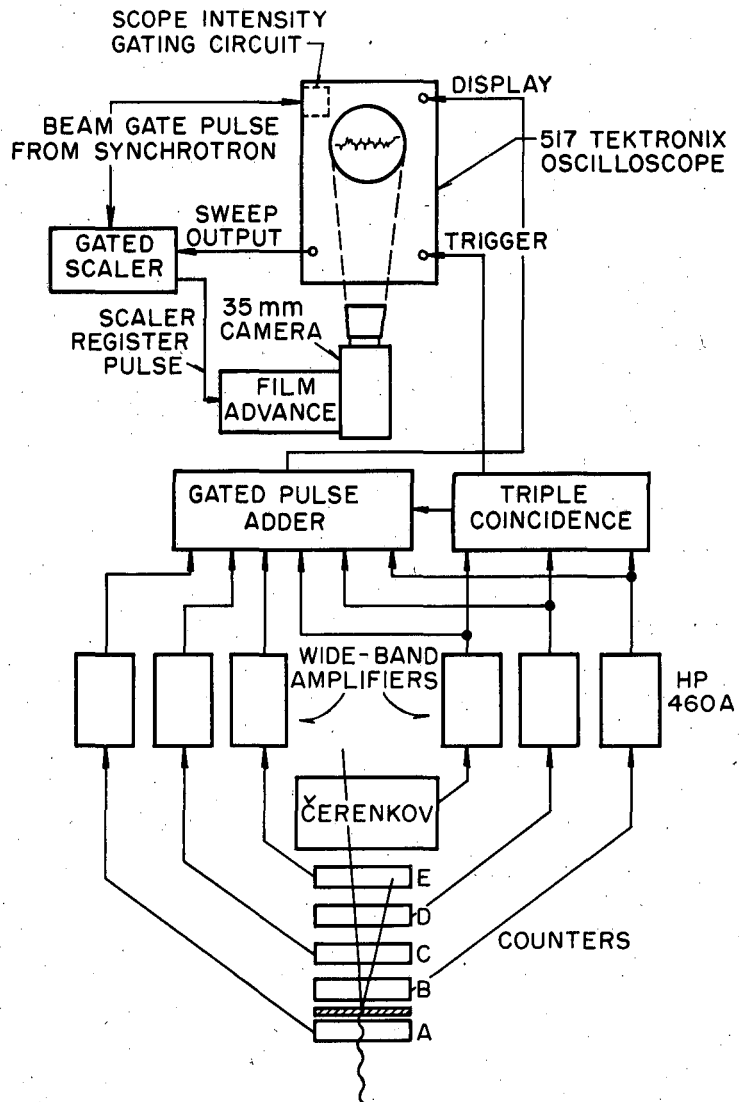
F. Electronics

A block diagram of the electronic equipment is shown in Fig. 9. A preliminary identification of gamma-ray events is made when an electronic triple coincidence is recorded between the B, D, and Cerenkov counters. Any pulses that were in the counters at the time of the triple coincidence are mixed together in the gated distributed pulse adder so that they may be displayed on the 517 Tektronix Oscilloscope. The pulse adder is gated on by a large pulse from the coincidence circuit. The coincidence circuit also triggers the 517 Tektronix Oscilloscope. A positive 20-volt 300- μ sec pulse is used to gate on the cathode ray beam in the oscilloscope and a scaler, which registers the number of sweeps, occurring at the beam spill-out time. An output pulse from the gated scaler triggers a relay circuit that automatically advances the film in the camera that records the events appearing on the oscilloscope.

Phototube high voltages were adjusted so that minimum-ionizing particles traversing the counters produce about 0.7-volt negative pulses, which are then connected with 125-ohm RG-63/U cable into terminated inputs of Hewlett-Packard 460 A wide-band amplifiers, and the approximately 5-volt output pulses are then sent into the pulse-mixing circuit and triple-coincidence circuit.

The A, B, C, D, and E counter elements of the gamma-ray telescope are plastic scintillation counters, each viewed by one 1P21 phototube operating at a typical high voltage of 1400 volts. The lucite Cerenkov counter is viewed by two RCA 6810 photomultipliers operating at about 1800 volts.

The triple-coincidence circuit is a simple Rossi parallel-type circuit. The schematic is shown in Fig. 10. The circuit takes unshaped input pulses of about 2 volts or more, is relatively fast (about 10^{-8} second time resolution), and provides a large output pulse (120 ma) with a fast rise time (10^{-8} second), which is very useful for triggering purposes and scaling. Because of the high input impedance to the coincidence circuit, the pulses that make



MU-13142

Fig. 9. Block diagram of electronic equipment.

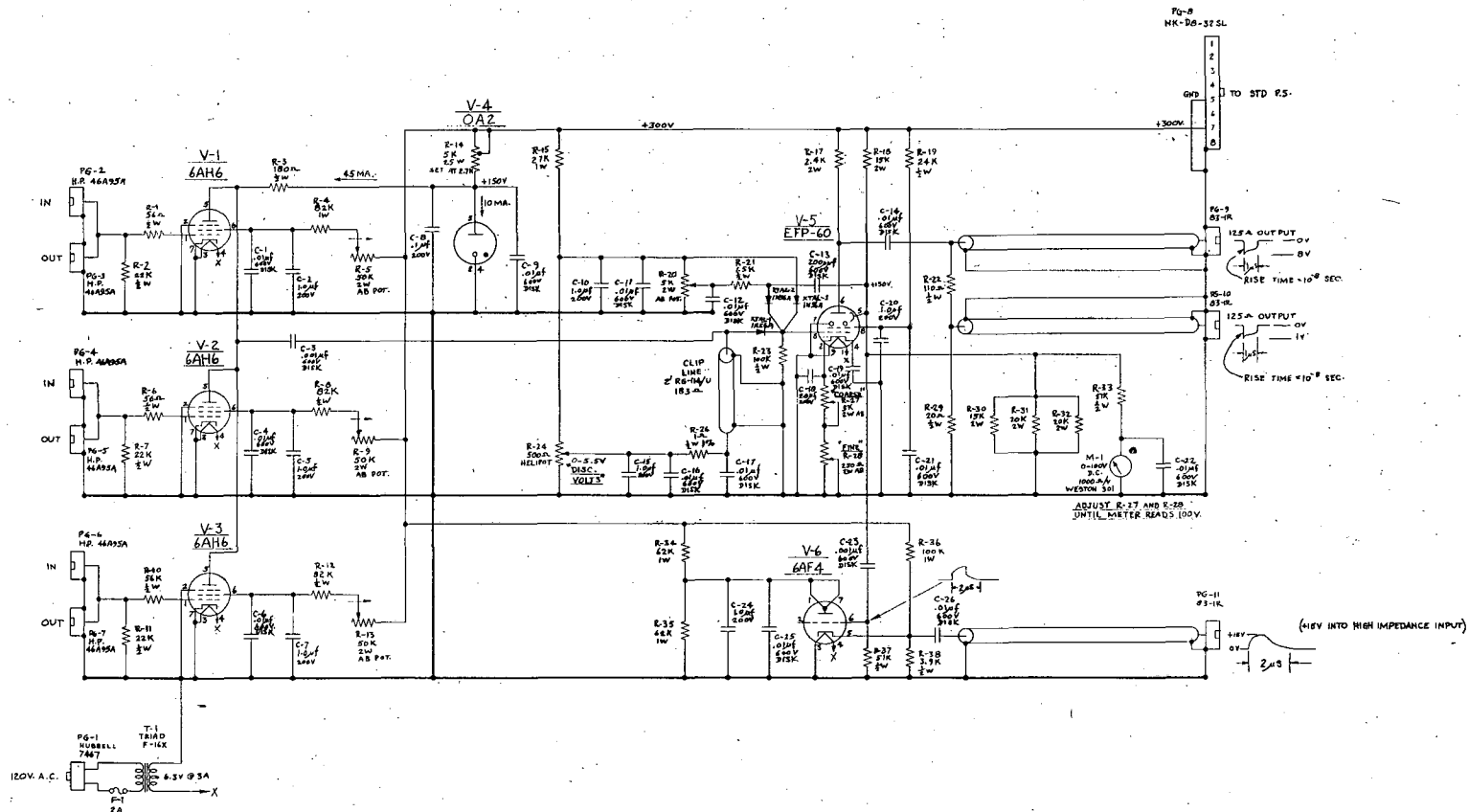
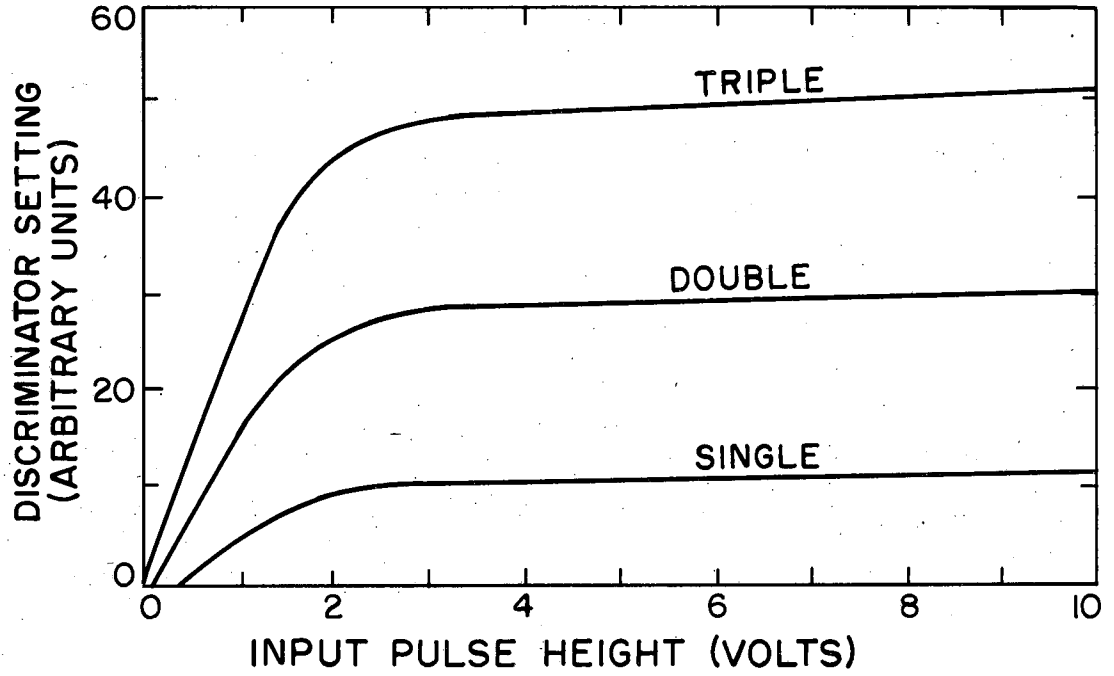


Fig. 10. Schematic of the triple coincidence circuit.

MUB-111

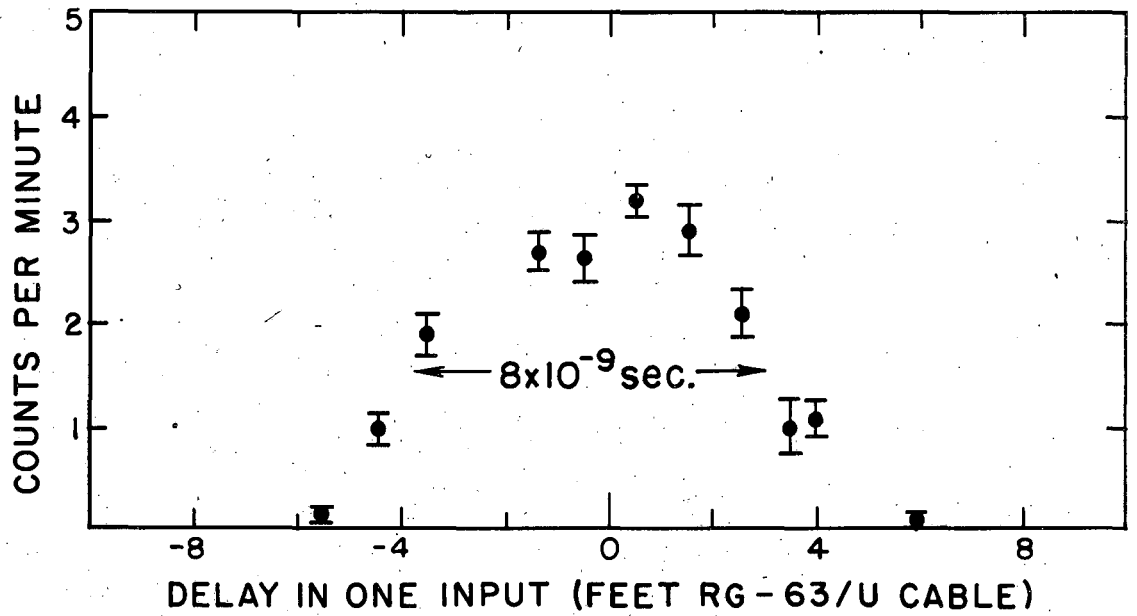
the coincidence may be photographed later without loss of rise time. Figure 11 shows how the order of the coincidence (triple, double, single) depends on the input pulse voltage and the discrimination level in the plate circuit of the 6AH6's. The doubles-to-triples ratio for phototube pulses is 50 to 1 when use is made of the limiting action of the HP 460 A amplifiers. The time resolution of the circuit was measured with cosmic rays. The delay curve is shown in Fig. 12. The half width at half-maximum time resolution is 4×10^{-9} second, and the counts drop to zero at 0.8×10^{-8} second. These figures are what would be expected from the clip line used (4×10^{-9} second clipping time). The long-time stability of the discriminator setting is 5% per day, and is accomplished by providing low-impedance biases for the diodes on back resistance, and large resistance values in the screens of the 6AH6's. Protection against charging effects under very high input counting rates is accomplished by clamping the dc voltage values with ample capacitors. The maximum allowable coincidence rate is one count per 5 microseconds, which is determined by the recovery time of the one-shot multivibrator output.

It is required to display, in a single sweep, the pulses from the six different counters on the 517 Tektronix oscilloscope at six different positions, so that the pulses may be identified without question as to which counter they originated in. To display a few counters at low counting rates, it is sufficient to merely add the pulses from the counters and delay them with respect to one another. The pulses are identified, then, merely by their position on the trace. For numerous counters and high counting rates, this simple means is not trustworthy, since accidental events on the trace lead to confusion in identification. To avoid this difficulty, the gated distributed adder was developed and is shown in Fig. 13. It has six input channels connected to a common output, but delayed with respect to each other by 8×10^{-8} second. All input channels are gated on, simultaneously, by a triple-coincidence event, for 8×10^{-8} second (1×10^{-8} second rise time and fall time). Replicas of the pulse that gated on each channel appear adjacent to one another in the



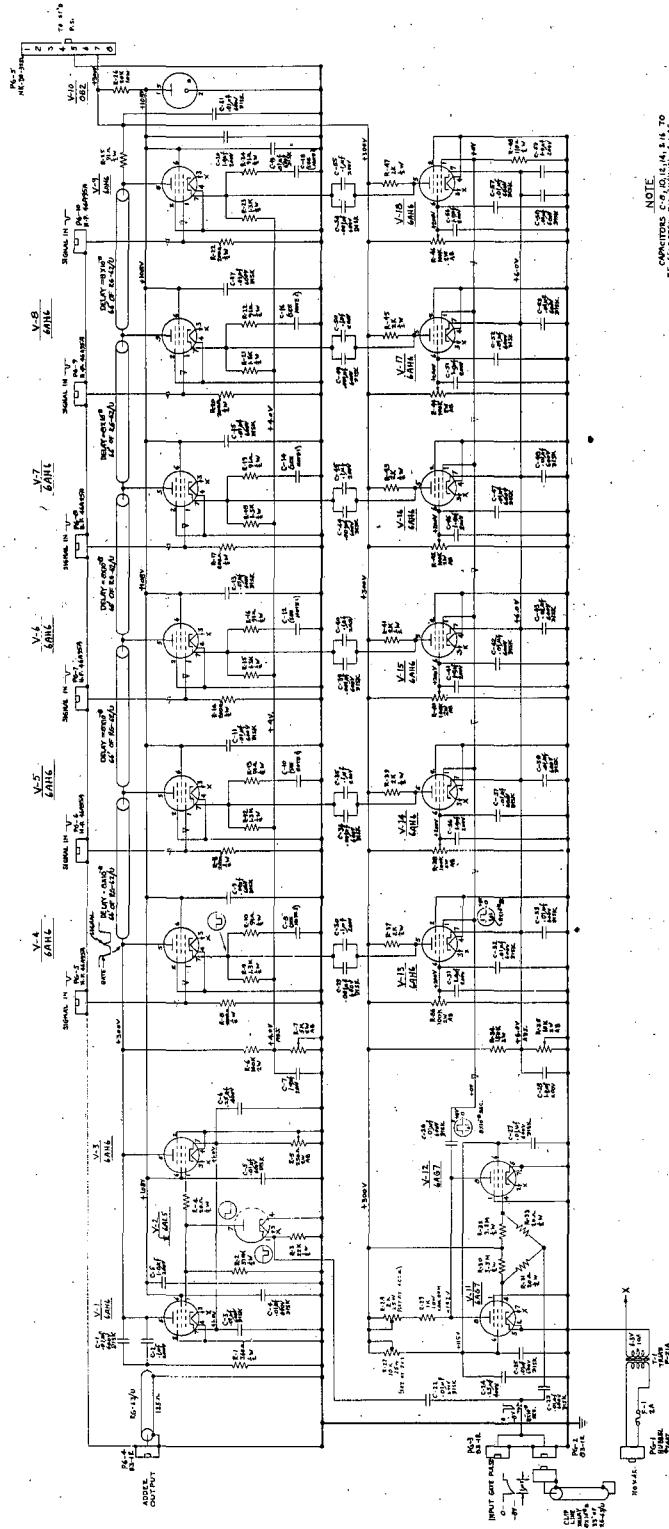
MU-13143

Fig. 11. Minimum discriminator setting versus input pulse height for a given coincidence multiplicity.



MU-13144

Fig.,12. Triple-coincidence time-resolution curve.



MUB-112

Fig. 13. Schematic of the gated distributed pulse adder.

output, since they are delayed with respect to one another by an amount just equal to the gating time. Since the oscilloscope is triggered and the adder is gated on by the coincidence pulse, and a given channel is open only at a specified time after the coincidence pulse, then the counter feeding that particular channel can appear only in one region on the oscilloscope trace after the coincidence pulse, and confusion in identification as to the origin of a pulse is eliminated. Thus, the position on the trace uniquely identifies the pulse. The replicas of the gate pulses appearing in the output are canceled out by a equal and opposite pulse. The rather strange-looking output of the gated distributed adder, described above, with input signals disconnected, is shown in Fig. 15a. The pulses that appear on this trace between the gates are due to imperfect adjustment of the positions of the gates and the gate widths. The over-all gain of the unit is about $1/4$.

In order to gate the counting equipment on only during the beam spill-out time (mainly to remove the cosmic-ray background), it was decided to leave all the equipment on, but to gate on the cathode-ray beam in the 517 Tektronix oscilloscope only. Since all the data were recorded photographically, this was sufficient to achieve the necessary gating. (The scalers are gated off, too.) The feature of gating the cathode-ray beam is not provided for on the 517 model, so that it was necessary to develop such a gating arrangement. The schematic of the circuit is shown in Fig. 14. The rise time to gate on the scope with this arrangement is about 1 microsecond. The unit requires a 20-volt gating pulse (from the scaler gate and beam monitor), and the proper setting is found by lowering the "intensity" knob so that when there is no gate pulse the traces are invisible. When the gate pulse arrives, the cathode-ray beam is gated on, to the usual intensity for photographing. The unit may be left on all the time, as it draws little current (1 ma), and the oscilloscope "intensity" knob is the only adjustment necessary.

G. Photographic Method

The decision to photographically record the scattering events was based on the necessity for conclusive identification of gamma rays at the low counting rates expected, in the presence of the high synchrotron background. A purely electronic means of selection to accomplish a short-time-resolution fivefold coincidence that is well plateaued and at the same time completely discriminative against fourfold or lower-order coincidences, and is protected against spurious counts even under the conditions of very high singles rates and low coincidence counting rates, is a difficult task at best. The photographic recording technique provides a solution in that all events are put to the ultimate visual test, and the requirements on the electronics are relaxed since they serve only the function of making a preliminary sorting. The price paid for this reliable means of identification is the many hours of time required to sort the desired events from those which do not fulfill the criteria set up for gamma-ray events.

The recording of an event is initiated by a triple coincidence in the B, D, and Cerenkov counters, which triggers a 517 Tektronix oscilloscope on which are displayed the pulses from the six counters of the gamma-ray telescope. The oscilloscope trace is photographed with a General Radio 35 mm oscilloscope camera which has been adjusted to focus the trace as a fine line on Kodak Linagraph Pan high-contrast film. The oscilloscope is set at a sweep speed of 100 $\mu\text{sec}/\text{cm}$, or about 1 μsec total sweep time and no deflections are allowed to exceed 1.1 cm on the cathode-ray tube. The film is automatically advanced about 3/8-inch for each event that occurs during the beam spill-out time. Events that occur outside this time, such as those due to cosmic rays, do not advance the film nor are they photographed, since the film-advancing mechanism and the cathode-ray beam of the 517 Tektronix oscilloscope are gated on only during the beam spill-out time. The maximum allowable repetition rate of the film-advancing unit is one event per two seconds. The film was developed and

ready for a preliminary scanning about two hours after a run. Examples of some of the events recorded are shown in Fig. 15.

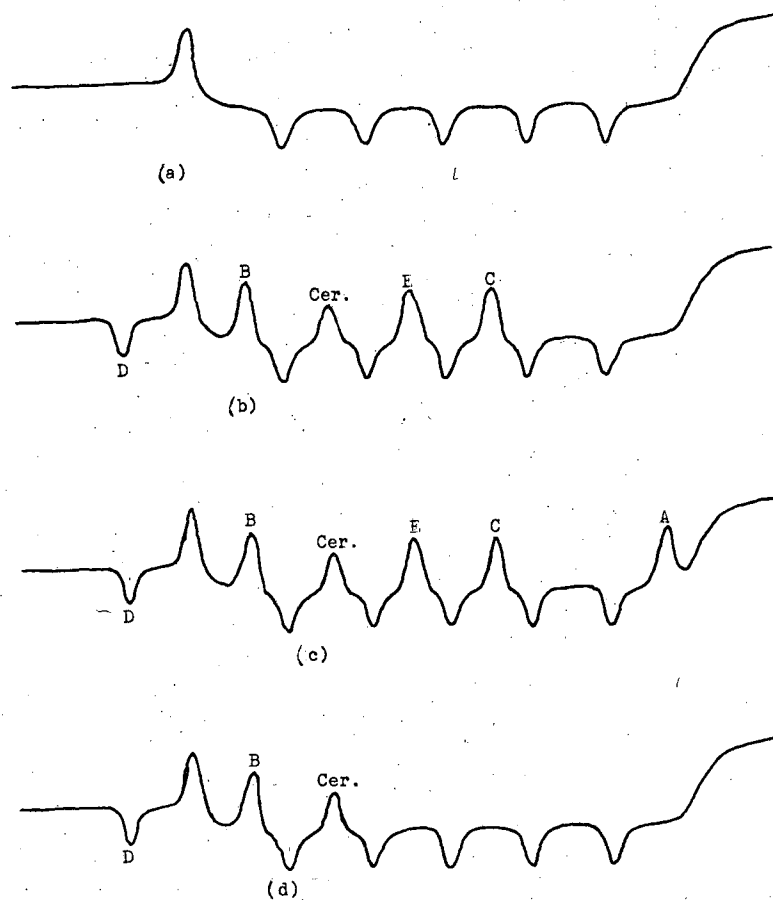
Example (a) is included to illustrate the output from the gated adder when the input pulses are disconnected, (b) is an event due to a high-energy gamma ray, (c) is a count due to an electron that registered a fivefold coincidence along with its anticoincidence pulse, and (d) is an event which involved only the B, D, and Cerenkov counters, which is sufficient to trigger the oscilloscope. It should be noted that the D pulse is not gated by the gated adder, and is displayed with negative polarity to avoid confusion with the other pulses.

Furthermore, the fifth input channel was not used, and the order of the pulses on the trace does not correspond to the order of the counters in their physical arrangement.

H. Experimental Procedure

The setting-up procedure consists of verifying that the axis of the beam is accurately lined up with the beam collimator system, and that the cross hairs of the transit are centered on the beam. Both the small lead collimator directly in front of the hydrogen target and the target itself are lined up by means of the transit cross hairs, and then their positioning is accurately checked with X-ray photographs of the beam; positioning thus is accurate to less than 1/16-inch. The gamma-ray detector is then located relative to the outer case of the target and measurements of the counter geometry are made.

The high voltage on each of the counters is adjusted so that the average pulse due to minimum-ionizing particles produces pulses at the coincidence circuit that are five times the minimum necessary to record a triple coincidence, and the discriminator of the coincidence circuit is adjusted just above the limit for double coincidences. Checks on the discriminator settings and phototube high voltages for plateaued conditions with cosmic rays were carried out, and an analysis of the film showed the equipment to be counting triple-coincidence events with high efficiency. Phototube high voltages, bias, and discriminator



MU-12984

Fig. 15. Oscilloscope traces.
(a) Gated adder output with input signals from counters disconnected.
(b) High-energy gamma-ray count.
(c) Electron count.
(d) Triple-coincidence event.

levels were checked frequently during the run, and a continuous check on the pulse height from the counters and the gain of the pulse adder and oscilloscope was obtained from the film data.

The running procedure consists of collecting data, for full-target and empty-target conditions, at three different synchrotron energies: 95, 113, and 132 Mev. These conditions were alternately cycled several times during the experiment, to minimize possible adverse effects due to long-time drifts. The energy of the machine and the beam spill-out conditions were monitored continuously by viewing an oscilloscope on which was displayed the output from a counter exposed to the direct synchrotron beam.

To verify that high-energy gamma rays were being counted, the converter-in/converter-out ratio was determined and found to be about seven, and a similar ratio was obtained for full and empty target. Several long runs to check for accidental events yielded negative results. A further test on the equipment was made by increasing the bremsstrahlung energy above the threshold energy for the photoproduction of neutral mesons, and a rapid rise in gamma-ray counting rate with machine energy was observed, due to the decay gammas from π^0 mesons.

I. Experimental Results

The experimental data that are obtained in this experiment consist of an accumulation of counts at three bremsstrahlung energies, which is the integrated result of the scattering at 90° weighted by the bremsstrahlung spectrum and the counter efficiency over the energy interval from about 40 Mev to the peak energy of the synchrotron. The net hydrogen-counting rates, corrected as discussed in Section III-D are as follows:

Synchrotron Energy k_m (MeV)	Counts per 10^{11} Equivalent Quanta
95	$6.68 \pm .42$
113	$10.16 \pm .51$
132	$14.59 \pm .64$

The cross section is obtained from these values by unfolding the bremsstrahlung spectrum and the dependence on energy of the counting efficiency. These calculations are carried out in Section III-E.

III. ANALYSIS OF THE DATA

A. Film Reading

The film data collected during the run are projected in a Recordak Film Reader for the analysis, and are examined for gamma-ray events, which are identified by a trace with pulses from the B, C, D, E, and Cerenkov counters that are larger than certain minimum pulse heights, all of which must fall at their expected positions within 6×10^{-9} second and not be accompanied by an anticoincidence pulse. The high-energy electron events are those which fulfill the condition for a real event but which include, in the proper position and larger than a certain minimum the anticoincidence pulse. Pulse heights are measured in the projector by means of a graph-paper scale (Keuffel and Esser 358-10.5L, 20 x 20 lines to the inch). A pulse-height unit is 1/20-inch, and 1 cm deflection on the cathode-ray tube corresponds to 37 units, or 4.7 cm in the film reader, so that the over-all gain of the camera and Recordak is 4.7. The Recordak enlarges the 35-mm film dimensions by a factor of 20. A 1-cm grid on the oscilloscope photographed at the start of each run and the perforations of the 35-mm film provided a means of checking possible shifts in over-all magnification of the equipment; however, no such changes were observed. The thickness of the trace, as seen in the projector, is 2.2 mm (0.47 mm on the CRT). The pulse-height measurements were reproducible to better than 4%.

The requirements that the pulses from each of the counters be larger than a certain minimum pulse height, which corresponds to setting discriminator levels in electronics, were carefully checked throughout the film reading by establishing the average pulse height due to minimum-ionizing particles in the counters so as to insure that these conditions remained the same in the scattering experiment and in the calibration experiment. It is essential that the film data be read the same way at all times, since the minimum pulse-height conditions directly influence the efficiency for gamma-ray detection.

Since the film was analyzed the same way in the calibration experiment and in the scattering experiment, the effect of the pulse-height minima is automatically included in the counter efficiency. It is estimated that the errors, in pulse-height measurements and in the fluctuation in the pulse-height minima, amount to 1% for all the data collected at each energy.

B. Background

A study of possible background contributions must, of necessity, be carried out rather extensively in an experiment of this type. Such a careful background analysis is necessary for several reasons: the cross section being measured is small (10^{-32} cm²/steradian); the method of detection identifies only the high-energy gamma rays scattered by hydrogen at 90° without a coincidence with the recoil proton, consequently one must be very sure that no other process could give rise to such high-energy gamma rays at large angles; and the experiment is subject to high background conditions, relative to the counting rates expected.

The discussion of background is restricted to bremsstrahlung energies below the threshold for neutral-meson production in hydrogen.

We are interested in those events in hydrogen, initiated by photons, each of which produces a high-energy photon at large angles, which is not due to the proton Compton effect. Of the two main processes taking place in hydrogen -- pair production and Compton electron effect -- only the latter yields a photon in the final state. As discussed earlier, the 90° -scattered quanta in the Compton electron effect are limited to an energy not exceeding one-half Mev, and in spite of the copious number of such events, they are not a troublesome background. Though pair production produces only a positron-electron pair and a slightly recoiling nucleus (proton), a higher-order process related to pair production can result in the production of a photon in the final state. The process is radiative pair production, or pair production followed by inner bremsstrahlung of one of the pair

electrons in the Coulomb field in which it was produced. It is possible for this process to produce high-energy photons at wide angles, since the ponderous proton can recoil with low energy to balance the large transverse momentum involved, contrary to the situation in the Compton electron effect and radiative triplet production. No theoretical treatment of this unlikely process is available, although information is obtainable on wide-angle pair production;¹⁴ consequently, to make a crude estimate of radiative pair production the cross section for the production of a high-energy pair electron at large angles is carried out, and then the extreme assumption is made that the electron is a gamma ray of the same energy as the electron. Under this assumption, in a calculation at a bremsstrahlung energy of 132 Mev, averaging the cross section over this spectrum and weighting by the counter efficiency, the effective cross section for this type of event is found to be $0.65 \times 10^{-32} \text{ cm}^2/\text{steradian}$, which is about 50% as big as the Thomson scattering cross section. However, the extreme assumption made is an overestimate by about a factor of 137, so that the contribution to the gamma-ray counting rate due to this process for 90° scattering angle is small. There is evidence from other laboratories that contributions due to this effect are apparent at small angles in the forward direction.

Multiple effects can now be considered. With the production of electrons in the hydrogen by the Compton electron effect and by pair production, other possibilities of background contributions are open. Electrons can produce high-energy photons directed towards the detector by wide-angle bremsstrahlung on protons, or the electrons incident on the detector can emit hard bremsstrahlen on passing through the walls of the target and the carbon absorber preceding the detector. A calculation of this electron flux, on the assumption that the Compton and pair electrons produced in the hydrogen are elastically scattered by protons to 90° , was made, and it accounted for about half the experimentally determined number of electrons, the other half presumably being due to wide-angle pair production and to electron

production in the air column and foils before the hydrogen target. With the experimental knowledge of the scattered electron flux, the number and distribution in energy of the electrons in the target can be calculated and consequently the wide-angle bremsstrahlung¹⁴ on protons may be evaluated, with the result: the contribution is less than 0.3%. The counts due to bremsstrahlung in the material before the counter are not negligible, and were determined at the three bremsstrahlung energies of this experiment from knowledge of the distribution of electrons impinging on the detector, the radiation cross section, and the counter efficiency. The magnitude of the correction is approximately 4% at each bremsstrahlung energy. Multiple scattering in hydrogen to 90° is negligible.

Preliminary experiments met with great difficulty because of the neutron background at the synchrotron. Experiments were carried out close to the machine for beam intensity, and since the experimental area is not shielded against the very high neutron background, the problem was acute. For example, a double-scintillator coincidence detector counts at a rate about a hundred times that expected for the proton Compton effect. Neutrons record such coincidences either by being fast and producing knock-on protons in each of the two scintillators or, as thermal neutrons, by capturing in the lead shielding and generating 7-Mev photons. Supposedly, these photons produce coincidences by multiple Compton electron events in the counters. The neutron background has made it necessary to use the high coincidence multiplicity of this experiment, and the Cerenkov counter eliminated the possibility of counts due to fast neutrons and their recoil protons. With this counter arrangement, contributions to the background counting rate by neutrons are small. Any counts that are possibly due to neutrons are subtracted out when the empty target counts are subtracted off.

High-energy proton counts are impossible because the absorber in front of the detector is thick enough to stop protons of the highest possible energy, and in any case, the anticoincidence counter

would reject them and the Cerenkov counter would not count them.

A background due to meson production on the deuterons in liquid hydrogen is possible because the momentum distribution of the nucleons in deuterium has the effect of lowering the threshold energy for meson production. Gamma rays originate in the production of meson -- in the case of neutral mesons -- through the two decay gamma rays and -- in the case of negative mesons -- by their capture in hydrogen. Positive mesons do not produce high-energy gammas. An evaluation of this background effect shows that it amounts to less than 0.5% compared with the proton Thomson cross section. It is small in spite of the large photomeson cross section, because there is little deuterium in liquid hydrogen (less than one part in 5000), the meson cross section is small near threshold, and only the tail of the deuteron momentum distribution provides collision energies above threshold.

Cosmic rays occasionally enter the gamma-ray detector at an angle such that they traverse only the five coincidence counters and not the anticoincidence scintillator. Events of this type appear as real counts, and occur at the rate of 107 counts per hour. These counts are practically eliminated by gating on the counting equipment only during the beam burst from the synchrotron. With the counting duty cycle of 0.0018, the cosmic-ray background is reduced to one count in 5 hours, which is a 3% correction to the 95-Mev data.

Counts due to accidental fivefold coincidences were found to be negligible. On the other hand, the accidental rejection of a real count by the anticoincidence counter was observed. This anti-accidental effect is evaluated by reading the film for anticoincidence pulses that do not appear in the proper position, and in view of the coincidence time resolution the correction is calculated to be 2% at the highest beam intensity.

The anticoincidence inefficiency is obtained from the pulse-height distribution of minimum-ionizing particles in the anticoincidence counter, and the minimum pulse height considered in the film reading. By this method the anticoincidence efficiency is found to be 98.0 % \pm 0.8%.

Since the number of electron counts amounts to about 30% of the real counting rate, this correction is less than 1%.

Finally, background effects that depend on whether the target is full or empty, or on whether the converter is in or out, may be considered. They are: (a) the background counts arising from the production in the walls of the target, and the general background of high-energy gamma rays in the synchrotron experimental area, both of which depend on the converter but not on the target; (b) the counts due to electrons that manage to scatter around the anticoincidence scintillator, or some other type of background that depends on the target but not on the converter, and (c) some sort of ambient background, such as high-energy electrons, gamma rays, or neutrons, which depends neither on the converter nor on the target.

The wall-scattering background (a) and the ambient background (c) are determined by runs with the target empty, and are subtracted from the full-target counting rate at each machine energy. The empty-target background is one-seventh of the total counting rate at 132-Mev and one-sixth at 95 Mev.

That the fivefold coincidence counts are really due to high-energy gamma rays is established by the marked dependence of the counting rate on the converter. On removal of the converter, the counting rate dropped by a factor of seven. The residual counting rate when the converter is out is compatible with the conversion in the first coincidence scintillator and the inefficiency of the anticoincidence counter (2%), which becomes important because the number of electrons that register a fivefold coincidence jumps by a factor of ten. In view of this fact, the unlikely background (b) above will be taken to be zero, and the converter-out counts are not subtracted from the main data.

The net hydrogen gamma-ray counting rates, corrected for the factors discussed in this section, are presented in the experimental results in Section II-I.

C. Bremsstrahlung Spectra

The calculation of the cross section depends on the knowledge of the distribution in X-ray energies in the bremsstrahlung beam. The spectra used in the calculation are due to Schiff,¹⁵ and represent the distribution of X-rays produced by a beam of monenergetic electrons striking an infinitely thin target. The distribution is obtained by integrating the Bethe-Heitler cross section over radiation-straggled electron angles and photon angles. The synchrotron X-ray target is platinum (Z = 78) and is 0.020-inch thick. The spectrum that has been averaged over photon angles is used instead of the 0° spectrum because the scattering of the electrons in the platinum target has the effect of sampling all angles of photon emission.¹⁶ The constant of the Schiff spectra has been taken to be 191. The analytic expression for the distribution of gamma-ray energies has been evaluated on the UCRL IBM 650 computer, and are shown in Fig. 16 for three synchrotron energies. The spectra have not been corrected for the spread in k_m due to the spread in beam spill-out time, since it only amounts to about 1 Mev. The Schiff spectra are denoted by $B(k_m, k)$ and are normalized to the same intensity at zero photon energy: $B(k_m, k) = 1.00$ for all k_m . With this choice, the spectra plotted in Fig. 16 correspond to about 2/3 of an equivalent photon; the exact value, Q, for each spectrum is given below:

k_m	Q
95 Mev	0.6731
113 Mev	0.6802
132 Mev	0.6864

Finally, the number of photons dn in the energy interval dk is

$$dn = Q(\exp) \cdot \frac{B(k_m, k)}{Q} \cdot \frac{dk}{k}$$

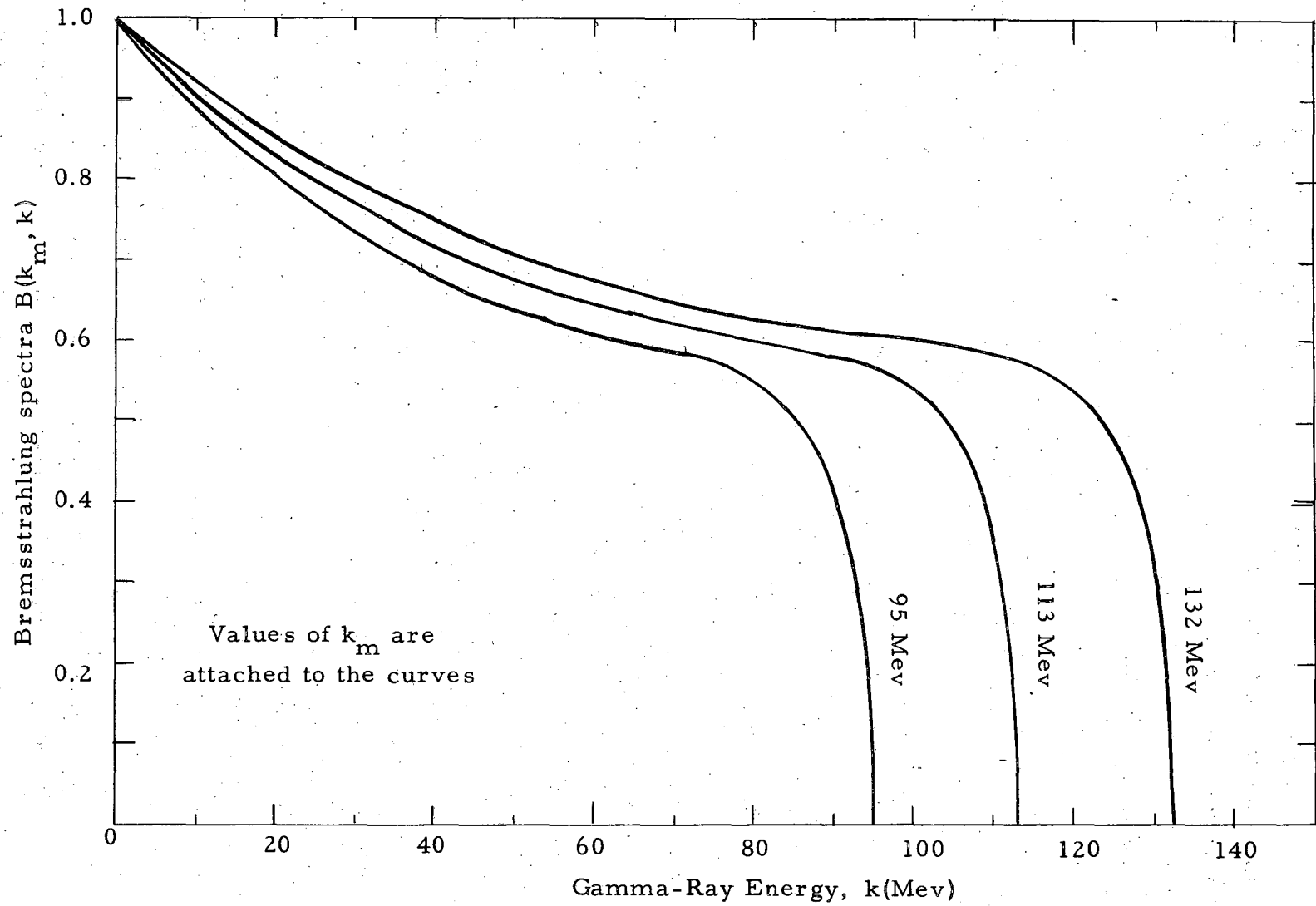


Fig. 16. Bremsstrahlung intensity distribution at three synchrotron energies.

where $Q(\text{exp.})$ is the number of equivalent quanta that have been incident on the target in an irradiation in the experimental area. Q is just the average value of $B(k_m, k)$ over the interval 0 to k_m . The spectrum B/Q is the X-ray intensity distribution normalized to one equivalent photon.

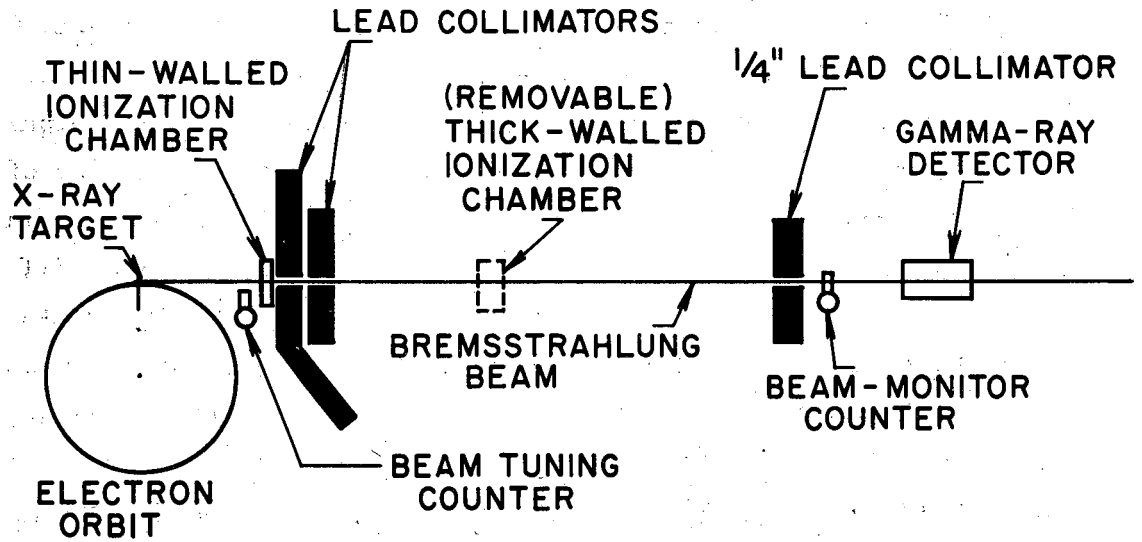
D. Gamma-Ray Detector Efficiency

It is of primary importance, in the calculation of the scattering cross section, to know the efficiency of the converter telescope for counting gamma rays. The efficiency for photons incident parallel to the axis of the counter has been measured by exposing the detector to the direct bremsstrahlung beam from the synchrotron; upon application of the photon difference method, the efficiency versus photon energy is obtained. In the actual scattering experiment, the gamma rays that are counted enter the detector at various angles of incidence and at various positions across the converter. The efficiency, as determined experimentally above, must be corrected for this effect of the finite size of the target volume and detector in their close physical proximity; a calculation is resorted to in evaluating this correction. In addition, consideration must be given to the effect on the gamma-ray efficiency of the Compton wave-length shift of the scattered quanta due to the recoil energy of the proton and of the loss of gamma rays resulting from the conversion in the materials before the detector. The fact that the detector has been calibrated in the bremsstrahlung beam is of fundamental value, since by this method the absolute beam-monitor sensitivity cancels out in the final cross-section calculation. The cross section is determined basically by the ratio of the counting rates in the direct and scattered beams, hence, only a relative beam monitor is required. Furthermore, by this technique, one automatically includes in the ultimate efficiency of the detector the effect of the lower pulse-height limit in the film analysis.

For the counter calibration experiment the detector was taken from its position at 90° to the beam line and swung around into the

direct beam of X-rays from the synchrotron and located at 256-inches from the source of X-rays. The pencil of gamma rays incident on the face of the converter was defined by a 1/4-inch-diameter lead collimator situated a short distance ahead of the detector, as shown in Fig. 17. Inasmuch as the detector is about 25% efficient for counting gamma rays, it was necessary to make a drastic reduction in the beam intensity for the satisfactory operation of the equipment in this arrangement. A reduction in beam intensity by a factor of 5×10^5 was required. To achieve workably steady beams at an intensity as low as this, which means the stable control of roughly 300 electrons in the synchronous orbit, a counter was located before the main collimation, and the integrated output per beam pulse was displayed on an oscilloscope for the tuning by the synchrotron operator. The low intensity was obtained by reducing the injector filament current and by badly misaligning the injector gun. A factor-of-100 reduction was also obtained by locating the counter at a considerable distance from the X-ray target and by collimating the beam to a fine pencil (0.25-inch diameter at 256 inches). No attempt to shape the beam pulse was made; the natural spill-out time of 10 to 20 microseconds' duration was used. The intensity incident on the detector through the 1/4-inch collimator was about half an equivalent quantum per beam pulse (3 Q per second). The efficiency measurements were made over the energy region of interest by varying the synchrotron energy from 40 to 174 Mev. To monitor the beam at low intensities, a single monitor counter was located in the beam after the 1/4-inch collimator, and was calibrated at various energies with respect to the thick-walled ionization chamber. The over-all error in the intensity reduction factor is $\pm 11\%$. The detector counting rate per equivalent quantum versus the machine energy k_m for central rays is shown in Fig. 18, it is denoted by $A_c(k_m)$ and is called the calibration activation curve. The activation data is related to the central counter efficiency, $\epsilon_o(k)$, by the relation

$$A_c(k_m) = \int_0^{k_m} \frac{B/Q}{k} \epsilon_o(k) dk,$$



MU-13145

Fig. 17. The experimental layout for the calibration of the gamma-ray detector by the photon-difference method in the direct synchrotron beam.

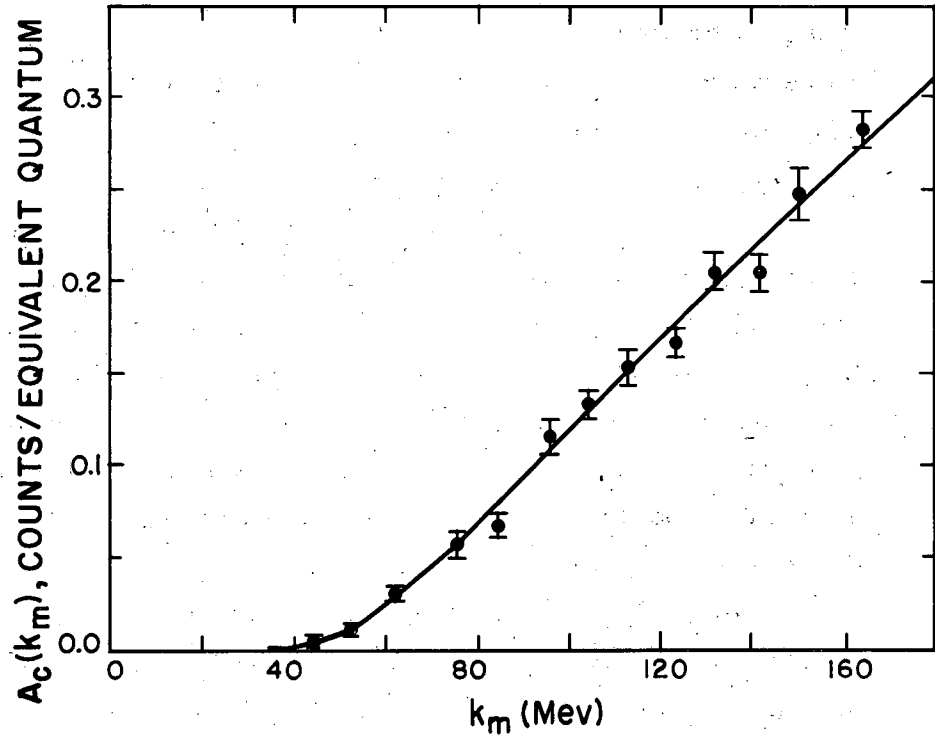
where B/Q is the bremsstrahlung intensity distribution for a peak energy k_m (normalized to one equivalent quantum). To solve this integral equation for the central efficiency, trial values of $\epsilon_o(k)$ were tested until an optimum fit was obtained with the $A_c(k_m)$ data in Fig. 18. The photon-difference method establishes the threshold energy and magnitude of the efficiency but not the detailed shape of the efficiency curve. Smooth curves for the shape of the efficiency as expected for a counter of this type were used. The calculations with the trial values of the central efficiency were carried out by assuming that $\epsilon_o(k)$ is constant over 10-Mev energy intervals below 100 Mev and constant over 20-Mev intervals above 100 Mev, and the number of photons in each of these intervals is determined from the bremsstrahlung spectra at various machine energies. By this method a set of linear equations is obtained which facilitates the calculation of the right-hand side of the above equation for various trial values of the central efficiency. The set of linear equations, for k_m ranging over the energy region considered, is

$$A_c(k_m) = \sum_{\bar{k}} \epsilon_o(\bar{k}) b(k_m, \bar{k}),$$

where the coefficients of $\epsilon_o(k)$ are

$$b(k_m, \bar{k}) = \int_{\bar{k} - \frac{\Delta}{2}}^{\bar{k} + \frac{\Delta}{2}} \frac{B(k_m, k)/Q(k_m)}{k} dk,$$

where \bar{k} is the mean energy in each interval of width Δ . These coefficients times 10^3 are listed in Table II. The measured best-fit central efficiency is shown in Fig. 19, and the activation curve appropriate to this efficiency curve is plotted along with the activation data of Fig. 18. It should be pointed out that the absolute efficiency depends on a knowledge of the sensitivity of the thick-walled ionization chamber.



MU-13146

Fig. 18. Activation data for the calibration experiment.

Table II. The coefficients $b(k_m, \bar{k})$ times 10^3 .

k_m (Mev)	\bar{k} (Mev)											
	35	45	55	65	75	85	95	110	130	150	170	
40	181
50	246	137
60	266	186	109
70	280	204	152	93
80	287	210	162	127	79
90	295	218	167	135	108	69
100	302	221	172	139	116	96	61
120	312	231	178	145	121	104	91	128
140	318	237	187	149	127	107	94	160	106	.	.	.
160	324	242	194	157	131	109	97	164	134	91	.	.
180	326	250	199	160	133	114	99	169	138	116	81	.

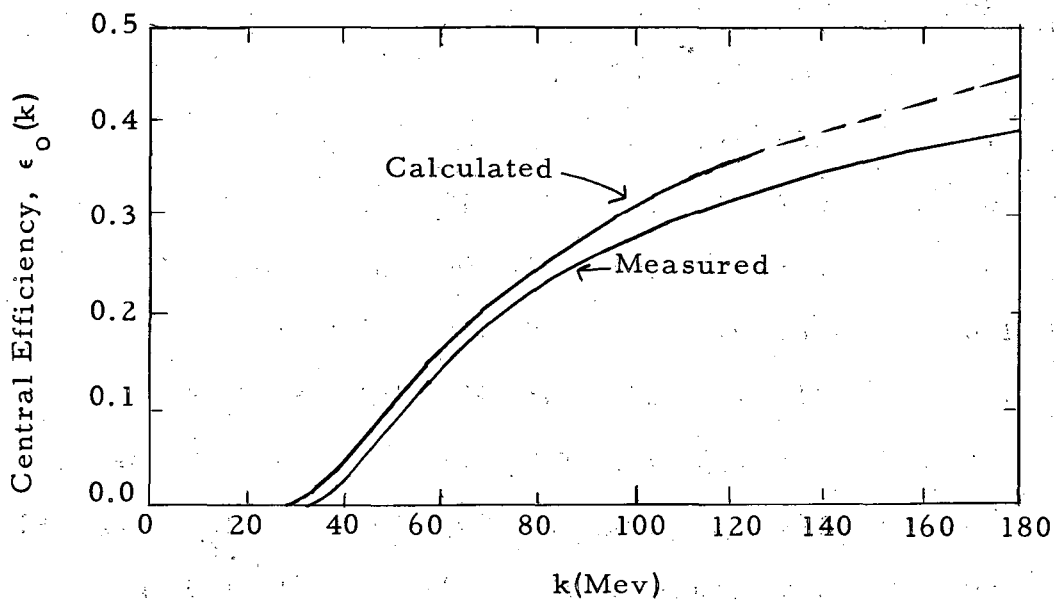


Fig. 19. Calculated and measured counter efficiency for central rays.

A calculation can now be made for the counter efficiency to estimate the effect of the actual experimental geometry. As the first step towards this, let us consider the general problem of calculating the efficiency of a gamma counter of this type in the case where the photons are incident at off-axis angles and at any position over the area of the converter. The counter is characterized by the area and thickness of the lead converter, the minimum energy to register a count (determined by the ionization loss in the counter material only), and the sensitive solid angular region subtended at each point on the converter in which, if an electron is emitted, it will register a count (provided its energy is great enough to penetrate all the coincidence counters). The actual efficiency of the counter of this experiment, then, is evaluated by averaging the efficiency described above over the angles of entrance into the counter and positions over the face of the counter for the particular geometry used. The angle of entrance into the gamma telescope is determined by the position in the target where the scattering took place and the point on the converter where the scattered gamma ray strikes. The limits of these angles are determined by the boundaries of the converter and the lead jaws which define the actual target volume of the liquid hydrogen. (See Figs. 6 and 7).

A general expression is now developed for the efficiency of a gamma ray telescope. Only the conversion in the lead converter is considered, and it is assumed to be all due to pair production. The thickness of the converter will be taken as 1/4-inch for all angles of entrance considered. That this assumption is a reasonable one is supported by the experimentally known fact that the efficiency of converter telescopes of this type is at a maximum with 1/4-inch-thick converters and thus are insensitive to small changes in the thickness of the lead. Furthermore, since we are mainly interested in the scattering, which varies as the square root of the thickness of the material, the variation of the characteristic scattering angle with thickness is gentle. In any case, the maximum variation in thickness encountered for the widest angles of entrance is only 8%. The

scattering distribution in angles of the individual pair electrons is assumed to be gaussian, and the $1/e$ scattering angle for the lead and counter material in series is compounded as a square root of the sum of the squares of the $1/e$ scattering angles in the two materials. The straggling in the radiation loss of the pair electrons in the lead converter will be treated as described by Heitler¹⁷ (p. 378). If E is the initial energy of an electron and E' is the energy of that electron (not including ionization loss) after traversing a thickness of material (lead), then the radiation straggling is described by the probability $p(\beta, y)$ that the electron will lose an energy $(E-E')$ due to radiation:

$$p(\beta, y) = \frac{(\ln \beta^{-1})^{a-1}}{\Gamma(a)}$$

where a is a number proportional to the thickness y of lead traversed ($a=1.62$ for $y=0.635$ cm), $\Gamma(a)$ is the gamma function, and $\beta=E'/E$. The probability distribution $p(\beta, y)$ is normalized:

$$\int_0^1 p(\beta, y) d\beta = 1.$$

The ionization loss of the electrons is assumed to be independent of energy (minimum ionization), and the fluctuation of ionization loss is not considered. The distribution in energy of the electrons in pair production is taken to be uniform between zero and the energy of the photon.

The probability that one of the pair electrons produced by a photon of energy k will register a count is

$$E(k) \cdot \Theta,$$

where

$$E(k) = \int_{y_L}^0 \exp\left(\frac{(y_L - y)}{y_0}\right) \frac{dy}{y_0} \int_{\lambda_{\min}}^1 d\lambda \int_{\beta_{\min}}^1 p(\beta, y) d\beta$$

and

$$\Theta = \int_R \bar{G}(\theta) d\theta d\phi.$$

This formula represents an average over the position in the converter, y , where the conversion took place (y_0 is the mean free path of a photon in lead, which is a function of energy k , y_L is 0.635 cm, and y is the distance in the lead measured from the back of the converter); an average over the partition energies, λk , of the pair electrons extending from the maximum energy $k(\lambda=1)$ to the minimum energy at the position y :

$$\lambda_{\min} = \frac{E_{\min}(y)}{k}$$

where $E_{\min}(y)$ is the minimum energy (ionization loss only) to register a count; and an average over the energies of the radiation straggled electron, the minimum energy necessary to traverse the rest of the counter determines the lower limit of the average: $\beta_{\min} = E_{\min}(y)/\lambda k$. The factor Θ is an integration over the angular region R determined by the sensitive volume of the detector as viewed from a particular position on the converter (the angle θ is measured with respect to the direction of the photon), and $\bar{G}(\theta)$ is the diffuse angular distribution of "eligible" electrons composed of a weighted average according to their physical distribution, over the variables y , λ , and β of the respective gaussian scattering distributions. An eligible electron is one which has at least enough energy to register a fivefold coincidence. The distribution $\bar{G}(\theta)$ is not gaussian and is normalized,

$$\int_0^\pi \int_0^{2\pi} \bar{G}(\theta) d\theta d\phi = 1.$$

In the calculation of the efficiency, it must be remembered that each of the pair electrons is potentially able to trigger the counter,

so that in reckoning the probability of counting a photon it is not merely the sum of the probabilities that each of the electrons will be counted, but also the usual law for adding independent probabilities, $P_1 + P_2 - P_1 P_2$, must be used. P_1 and P_2 are the probabilities of the respective pair members' registering a count. The efficiency obtained so far for counting a photon, $2E(k)\Theta$, must then be corrected by a second-order term which is closely approximated by

$$\chi(k) \cdot \Theta^2,$$

where

$$\chi(k) = \int_{y_L}^0 \exp\left(\frac{y_L - y}{y_0}\right) \frac{dy}{y_0} \int_{\lambda_{\min}}^1 d\lambda B(\lambda, y) P(1 - \lambda, y)$$

and

$$P(\lambda, y) = \int_{\beta_{\min}}^1 p(\beta, y) d\beta, \quad \beta_{\min} = \frac{E_{\min}(y)}{\lambda k}$$

The expression is approximate because Θ^2 is used to represent the second-order scattering factor. Several examples were tested and show that this is a good approximation (less than 10% error in the cross term). The approximation to the second-order term is exact if Θ is equal to one. The cross term becomes of negligible importance when the efficiency of the counter is low (relative to the maximum possible efficiency, i. e., about 50%). Finally the efficiency for counting a photon of energy k incident on the counter at some angle and at some position on the converter (the dependence on these variables is contained in the factor Θ) is

$$\text{eff.} = 2E(k) \cdot \Theta - \chi(k) \cdot \Theta^2.$$

Before this formula may be used, the average angular distribution of eligible electrons, $\bar{G}(\theta)$, must be evaluated somehow. To accomplish this, a Monte Carlo calculation was used to evaluate the distribution in 1/e scattering angles of emergent electrons for a photon of particular energy. A Monte Carlo calculation was appropriate because of the very cumbersome expression of the composite 1/e scattering angle for the lead and counter materials in series, which depends on the depth y in the converter, the energy of a pair electron at the time of its creation, $E = \lambda k$, and its energy after traversing the remaining lead, $E' = \beta E$ (not including ionization loss). The Monte Carlo calculation consisted of choosing the three variables y , E , and E' (or y , λ , and β) according to their physical distributions and then with these three variables calculating the composite 1/e scattering angle for each particular event. According to the usual Monte Carlo technique the three variables were chosen according to their physical distributions by choosing values of their integral distributions at random. Sixty calculations of the 1/e scattering angles were made at several photon energies, and with their corresponding gaussian scattering distributions the over-all angular distribution $\bar{G}(\theta)$ could be evaluated. It should be noted that this final distribution is not gaussian, and refers to only the eligible electrons at each photon energy. The width of these distributions varies approximately as $1/k$. Distributions are shown in Fig. 20. With $\bar{G}(\theta)$ it is possible to calculate the efficiency for counting a gamma ray at energy k which enters at an arbitrary position on the converter, if the angular limits relative to the direction of the photon of the sensitive volume of the counter are known.

Armed with this means of calculating the efficiency, one can evaluate the factors that enter in the final cross section calculation. The liquid hydrogen target volume will be approximated by a line source; the distance from the center of the target along the beam axis is denoted by x . The experimental geometry considered in this calculation is shown in Fig. 6 and 7. The effective target length L and the efficiency times solid angle $\Omega \epsilon$ which appear in Section III-E on

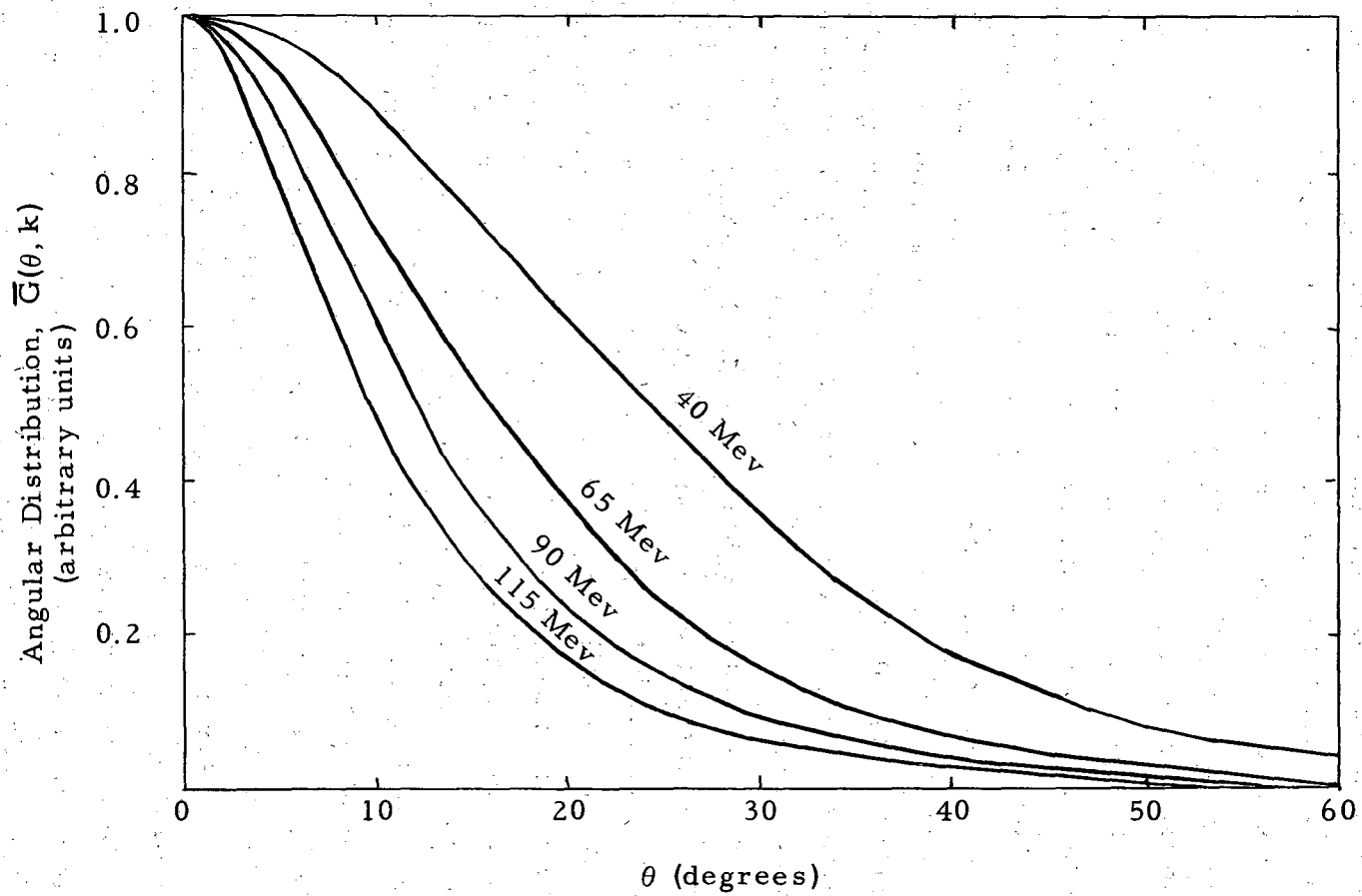


Fig. 20. "Eligible" electron angular distribution at various photon energies.

the cross-section calculation are expressed in the relation

$$L \Omega \epsilon = \int_{-\infty}^{\infty} \int_{\text{converter}} (\text{eff.}) d\Omega dx,$$

where

$$\text{eff.} = 2 E(k) \cdot \Theta - \chi(k) \cdot \Theta^2.$$

The integral represents an average of the detector efficiency over the length of the target, x , and the average over the surface of the converter weighted by the solid angle of the converter subtended at the position x . The efficiency in the actual counter geometry is normalized to the experimentally measured efficiency of the counter for central rays by

$$\epsilon_o(k) = \frac{[2 E(k) \Theta - \chi(k) \Theta^2]_{\text{Experimental Geometry}}}{[2 E(k) \Theta - \chi(k) \Theta^2]_{\text{Central Rays}}}$$

The expression in the denominator is the calculated central efficiency shown in Fig. 19. The efficiency times solid angle at a particular value of x is

$$\epsilon(x) \Omega(x) = \int_{\text{Converter}} (\text{eff.}) d\Omega$$

and

$$L \Omega \epsilon = \int_{-\infty}^{\infty} \epsilon(x) \Omega(x) dx.$$

Here $\Omega(x)$ is defined as the solid angle of the converter subtended at x , and includes the collimation by the lead jaws that define the counter aperture; $\Omega(x)/\Omega(0)$ is shown in Fig. 21. $\Omega(0) = 0.198$ steradian. Also shown in this figure is $\epsilon(x)/\epsilon(0)$. The effective target length L of the liquid hydrogen target is defined as

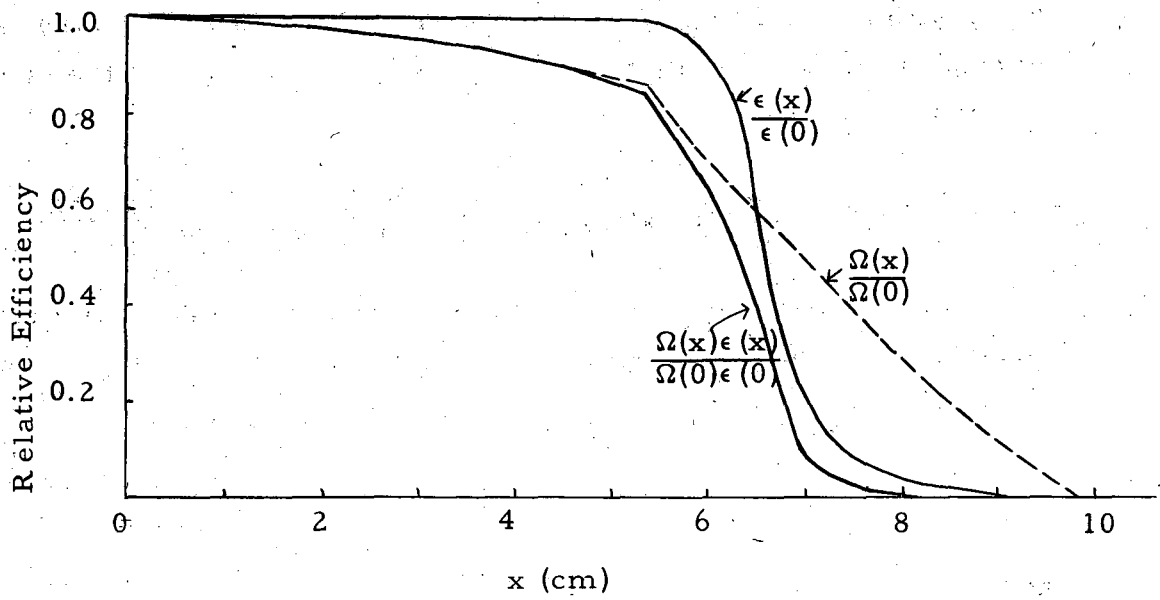


Fig. 21. Weighting factors as a function of position in the target.

$$L = \int_{-\infty}^{\infty} \frac{\epsilon(x)}{\epsilon(0)} \cdot \frac{\Omega(x)}{\Omega(0)} dx = 12.0 \text{ cm.}$$

The counting rate from the various target positions, x , is weighted by $\epsilon(x)\Omega(x)$, which is also shown in Fig. 21. With this choice of the effective target length, then we have

$$\Omega \epsilon = \Omega(0) \epsilon(0).$$

Though this choice of the definition of L is arbitrary, of course, the quantity $L \Omega \epsilon$, which determines the cross section, is not arbitrary.

The solid angle times efficiency is finally modified by

(a) The loss of gamma rays by conversion in the material before the detector. This loss amounts to about 15%, and it is virtually independent of the angle at which the photons traverse the materials to enter the detector.

(b) The shift in scattered gamma-ray energy due to the recoil proton amounts to evaluating the efficiency at k' instead of k where $k' = k/1 + \frac{k}{Mc}^2$. The correction amounts to about a 10% reduction in counting efficiency.

The solid angle times efficiency, averaged over the experimental geometry, and corrected for losses in the material preceding the detector and for the proton recoil, is denoted by $\Omega \epsilon'$ and is plotted in Fig. 22. This is the quantity that appears in the final cross-section calculation.

The differential cross section versus scattering angle is weighted by the relative angular aperture of the detector, $a(\theta)$, which is proportional to the counter efficiency at a given value of θ averaged over the length of the target,

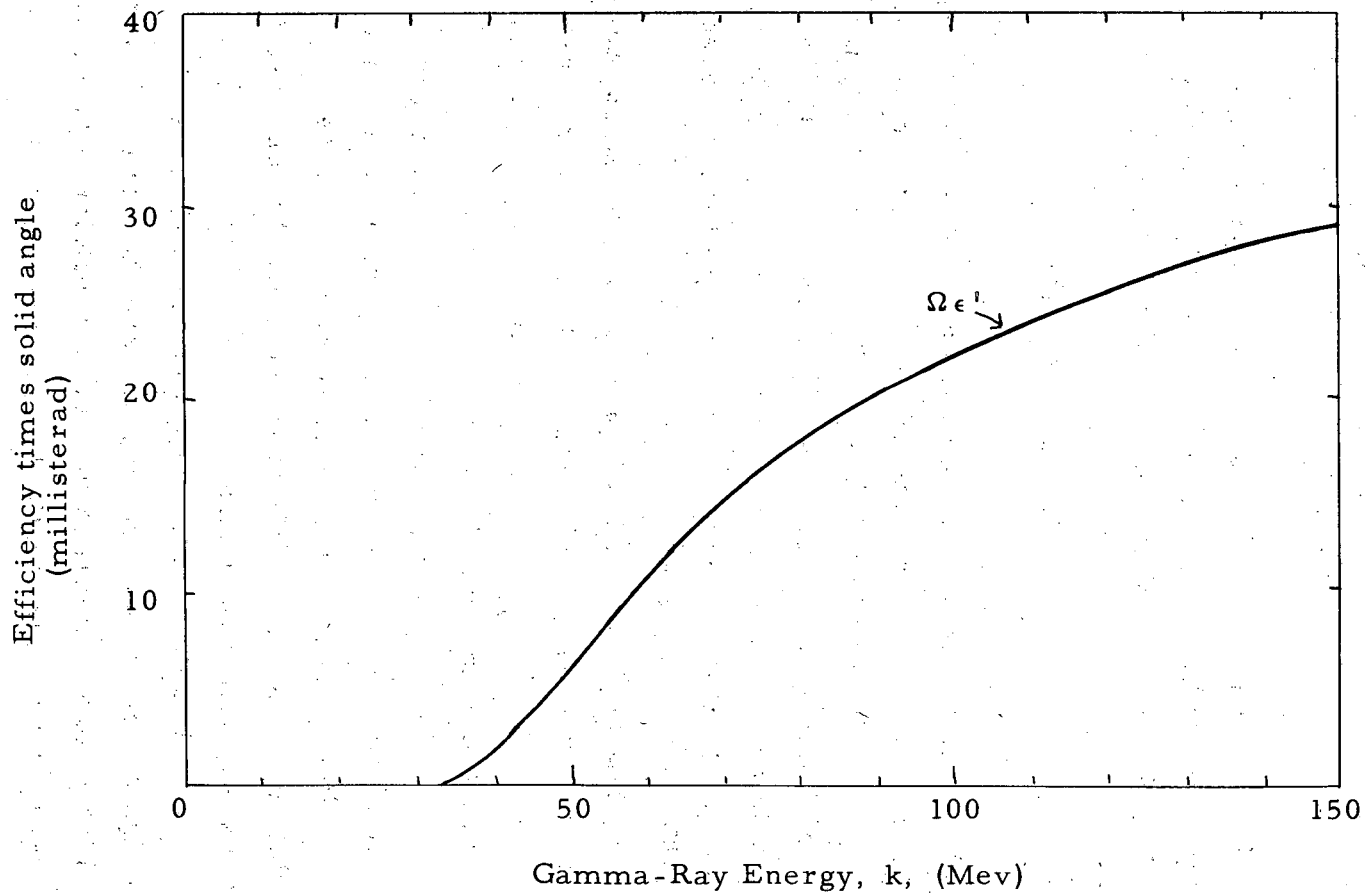


Fig. 22. Efficiency times solid angle of counter telescope in experimental arrangement.

$$a(\theta) \sim \int_{-\infty}^{\infty} \Omega(x) \text{ eff. } (\theta) dx,$$

and $a(\theta)$, normalized so that $a(90^\circ) = 1$, is shown in Fig. 23. As a first approximation the scattering cross section is assumed to depend on angle as the Thomson cross section, $1 + \cos^2 \theta$. Averaging this function over the effective angular aperture centered at 90° , one obtains

$$\frac{\int_0^\pi (1 + \cos^2 \theta) a(\theta) d\theta}{\int_0^\pi a(\theta) d\theta} = 1.037.$$

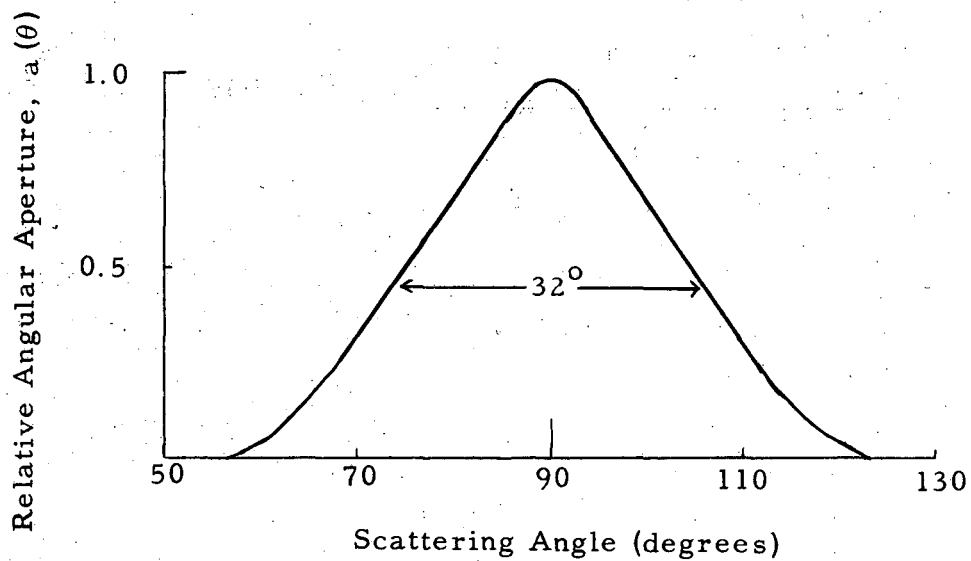


Fig. 23. Counting efficiency versus scattering angle.

E. Calculation of the Cross Section

The net liquid hydrogen gamma-ray counts per equivalent quantum, $A(k_m)$, for a peak bremsstrahlung energy of k_m , is called the activation curve. It is related to the scattering cross section in the following way:

$$A(k_m) = nL \int_0^{k_m} \frac{B/Q}{k} \frac{d\sigma}{d\Omega} \Omega \epsilon' dk,$$

where n is the number of protons/cm³; L is the effective target length, B/Q is the bremsstrahlung intensity distribution for a peak energy k_m (normalized to one equivalent quantum); $\frac{d\sigma}{d\Omega}$ is the differential cross section for photons of energy k , which has been averaged over the angular aperture of the detector centered at 90°; and $\Omega \epsilon'$ is the efficiency times solid angle of the counter telescope averaged over the experimental geometry. The prime signifies that it has been modified by the shift in the scattered gamma-ray energy due to the recoil of the proton, and corrected for the loss of counts in the materials before the detector. The experimentally determined values of $A(k_m)$ are given in Section II-I on experimental results.

At each machine energy, k_m , the differential cross section as a function of energy, $\frac{d\sigma}{d\Omega}$, is weighted by the function $\frac{B/Q}{k} \Omega \epsilon'$, which is the bremsstrahlung photon distribution modified by the counter efficiency, which cuts off the lower part of the spectrum. These weighting functions are shown in Fig. 24. The experimentally determined values of $A(k_m)$ and the activation curves expected for the Thomson, Klein-Nishina, and Powell cross-sections are shown in Fig. 25.

The photon difference method is used to get the cross section at a particular energy. To carry out this calculation the cross section is assumed to be constant over three energy intervals: (a) 40 to 95 Mev, (b) 95 to 113 Mev, and (c) 113 to 132 Mev. The relation between the activation data points and the cross sections in these intervals is contained in three linear equations:

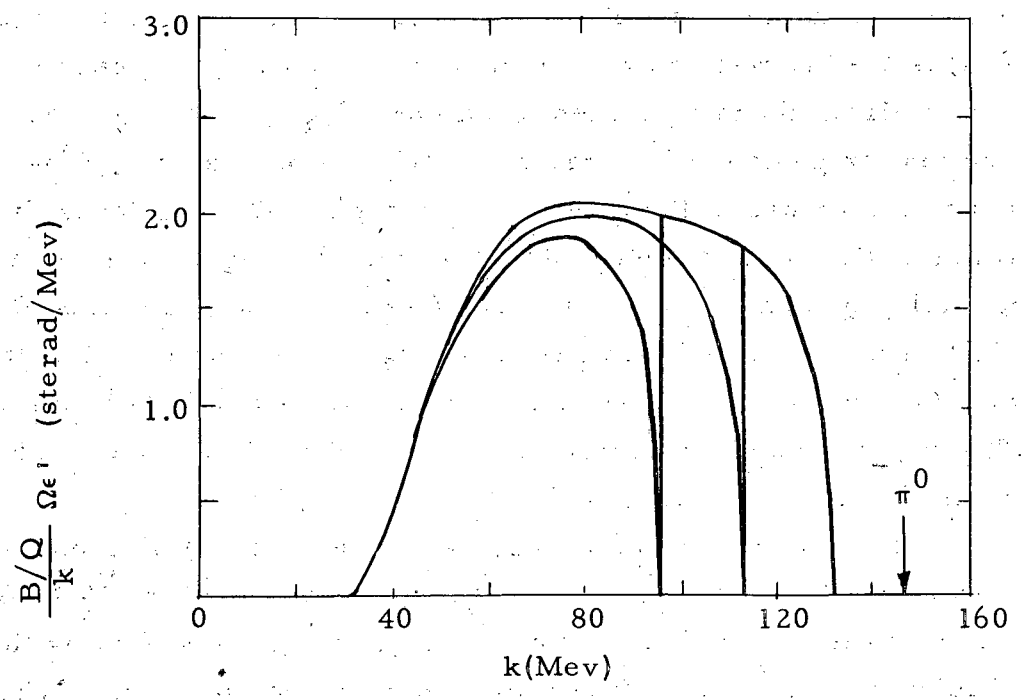


Fig. 24. Cross-section weighting functions.

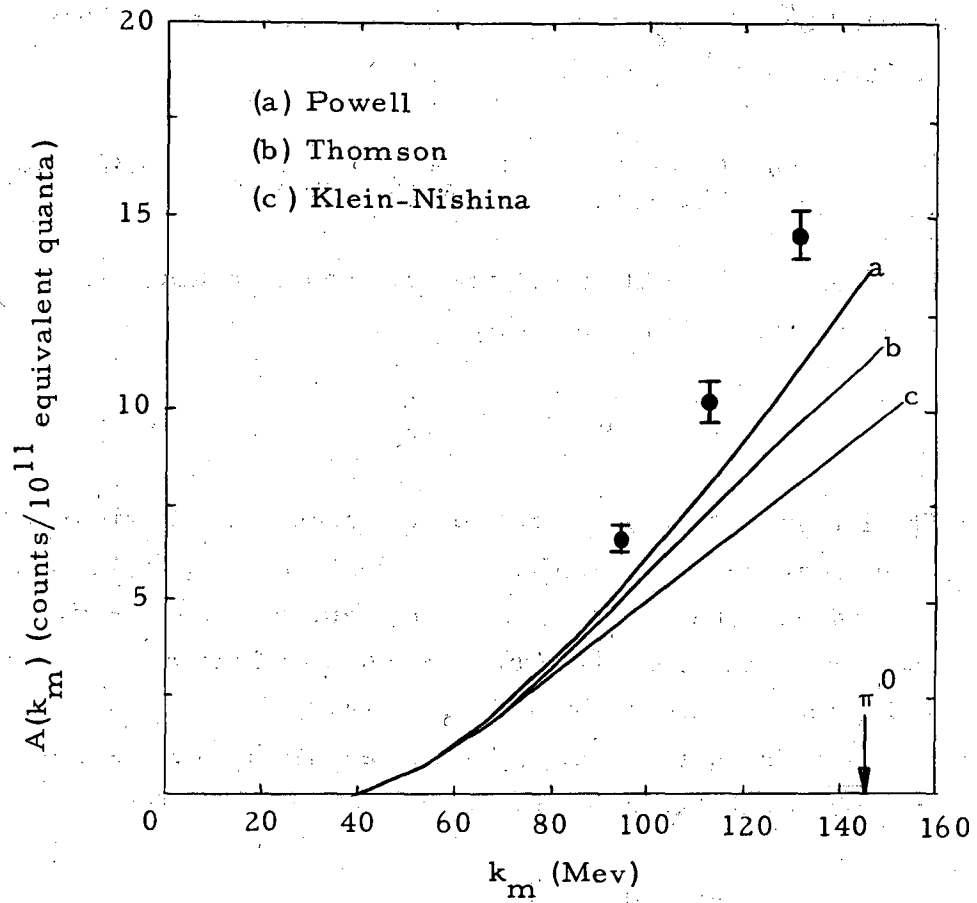


Fig. 25. Activation curve.

$$10'' A(95 \text{ Mev}) = A_1 = 5.05 \sigma_1,$$

$$10'' A(113 \text{ Mev}) = A_2 = 5.68 \sigma_1 + 1.64 \sigma_2,$$

$$10'' A(132 \text{ Mev}) = A_3 = 5.90 \sigma_1 + 2.15 \sigma_2 + 1.72 \sigma_3.$$

The differential cross sections in the intervals defined above are denoted by σ_1 , σ_2 , and σ_3 , and are in units of the Thomson differential cross section at 90° :

$$\left. \frac{d\sigma}{d\Omega} \right|_{\text{Thomson}}^{(90^\circ)} = \frac{1}{2} \left(\frac{e^2}{Mc^2} \right)^2 = 1.18 \times 10^{-32} \text{ cm}^2/\text{steradian}.$$

The numerical coefficients are obtained by evaluating, in the respective energy intervals, the quantity

$$nL \cdot 1.037 \cdot \frac{1}{2} \left(\frac{e^2}{Mc^2} \right)^2 \int \frac{B/Q}{k} \Omega \epsilon' dk.$$

The integral is proportional to the areas of the regions bounded by the weighting functions and the vertical lines in Fig. 24. The factor 1.037 follows from an average of the differential cross section over the aperture of the detector (the dependence of the cross section on scattering angle is assumed to be $1 + \cos^2 \theta$).

The solution of the linear equations for the cross-section values in terms of the activation data is

$$\sigma_1 = 0.198 A_1,$$

$$\sigma_2 = 0.602 A_2 - 0.679 A_1,$$

$$\sigma_3 = 0.581 A_3 + 0.169 A_1 - 0.756 A_2.$$

The errors in each of the cross section values are obtained as the square root of the sum of the squares of the fluctuations of the terms in each equation, due to the errors in the activation data points, $A(k_m)$.

The cross-section values obtained are

$$\sigma_1 = 1.32 \pm .08,$$

$$\sigma_2 = 1.58 \pm .42,$$

$$\sigma_3 = 1.92 \pm .54.$$

These results are plotted in Fig. 26.

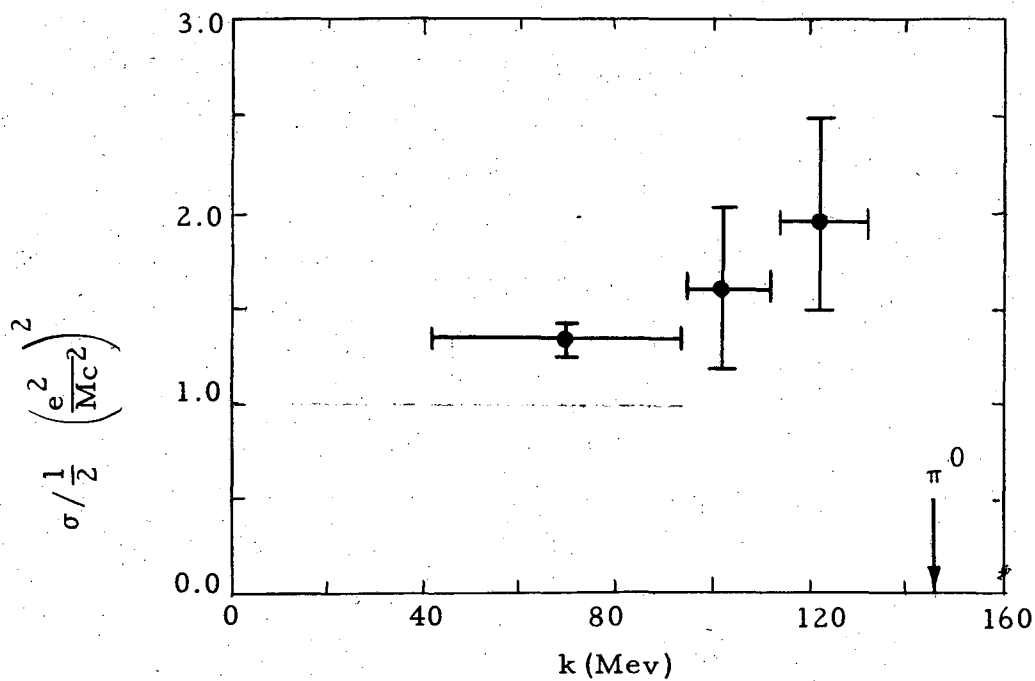


Fig. 26. The differential cross-section values obtained from the photon difference calculation.

IV. RESULTS

A. Discussion of the Results

As the cross section is expected to be nearly the Thomson value in the low-energy region of this experiment, the experimental results are considered high. The high values are apparent at each point of the activation data, and hence, in the cross section values. The discrepancy seems to be uniform with energy and amounts to about 30%, which, if it is compared with the Powell cross section, is well outside the counting-statistics errors of the activation data. It is felt that this discrepancy must be attributed to a constant-factor error at each experimental point. This supposition can now be considered in the light of the experimental techniques used.

It is believed that this discrepancy cannot be attributed to an error in the counter efficiency. Inasmuch as the detector was calibrated in the beam relative to the same beam monitor as was used in the scattering equipment, an error in the absolute value of the beam-monitor sensitivity would cancel out in the final result. Actually, this is true only if the sensitivity of the beam monitor is independent of energy. The beam-monitor sensitivity is a slowly varying function of the bremsstrahlung energy, and the fact that the calibration experiment was carried out at energies overlapping those of the scattering experiment minimizes any errors of this origin. Further, since the measured and calculated efficiencies are in good agreement, the error introduced by the energy dependence of the beam monitor on energy appears to be small. The calculation to modify the central counter efficiency to that of the actual experimental geometry is considered an accurate modification and, in any case, it is only a calculation of a correction to the over-all efficiency, so that an error in this correction has a relatively small effect on the over-all efficiency. An error in the determination of the synchrotron energy should be of small importance in the magnitude of the final cross section, as it affects the calibration data and scattering data in roughly the same

way, hence tends to cancel out in the final result. Since the error seems to be the same at each energy, one might suspect errors in the solid angle subtended by the counter (which is sensitive to the distance between the target and detector in the close geometry of this experiment) or in the effective target length, or some systematic error in the calibration experiment in stepping down the beam intensity by a factor of almost a million (statistical errors of 11% are expected).

To check the absolute value of the cross section, neutral-meson data were collected and compared with the experimentally known cross section for neutral-meson production. At the end of this experiment, the synchrotron energy was raised above the threshold energy for meson production, and counting rates were obtained at energies up to 200 Mev, where experimental data are available on the π^0 cross section. The comparison was made with the data of Mills.¹⁸ As the experimental arrangements of the two experiments were similar, it was possible to make a direct comparison between the neutral-meson activation data instead of comparing the actual π^0 cross section, with due consideration of the differences in solid angle, counter efficiency, and target volume. In the comparison, a small interpolation of Mills' data from 84° to 90° was required, and in comparing the efficiencies, both experiments were subject to the same assumptions concerning the averaging of the counter efficiency over the decay gamma-ray spectrum from neutral mesons produced in hydrogen. The result of this comparison shows again that the data of this experiment are high. If the π^0 activation data of this experiment are divided by the factor that is necessary to normalize the observed elastic-scattering cross section to the value expected at 70 Mev (1.24), then agreement is obtained, within the statistics of the measurements, with the π^0 data of Mills.

It is concluded that the data are high because of some error factor that is independent of energy and independent of the process being observed, whether it be elastic scattering or photoproduction of neutral mesons.

The cross-section data are normalized to the expected cross section at 70 Mev and shown in Fig. 27, ready for a comparison with theoretical expectations. The data at each energy have been divided by a common factor of 1.24.

B. Comparison With Theory

The scattering cross section is given as the square of a scattering amplitude, which is composed of individual terms which originate in the various types of interactions that give rise to the scattering of gamma rays. It is easier to study these contributions by studying the scattering amplitude rather than the scattering cross section, since, on squaring, the respective terms are mixed because of interference, and the resulting expression is not readily analyzed for physical significance.

The basic unit of cross section for the scattering of gamma rays by protons is:

$$\left(\frac{e^2}{Mc^2}\right)^2,$$

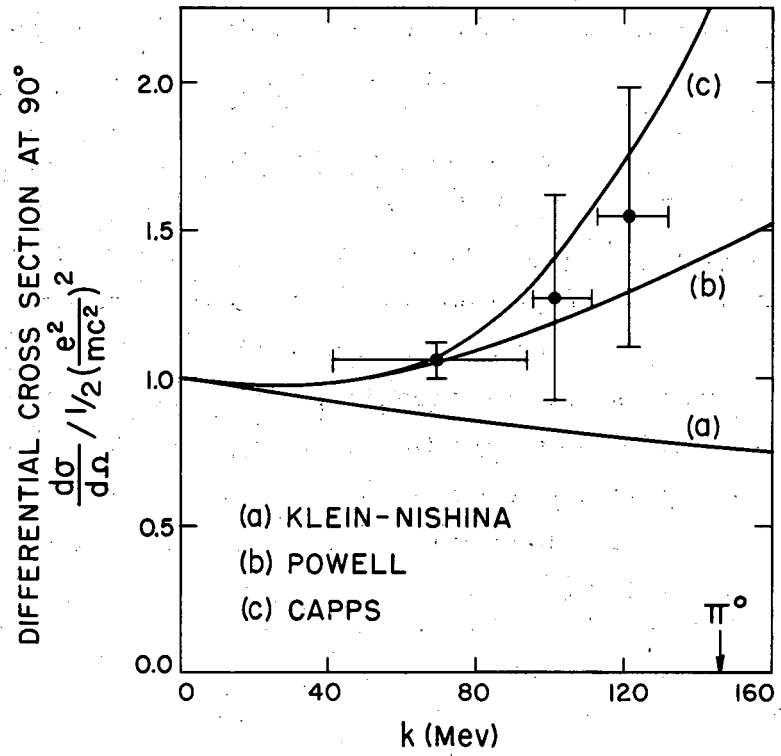
which is understood in terms of the proton Thomson scattering. The proton Thomson scattering amplitude is

$$\left(\frac{e^2}{Mc^2}\right) (\hat{e} \cdot \hat{e}'),$$

where \hat{e} and \hat{e}' are unit vectors in the direction of the polarization of the primary and scattered quanta. The Thomson scattering cross section is given by

$$\frac{d\sigma}{d\Omega} \text{ Thomson} = \left(\frac{e^2}{Mc^2}\right)^2 |\overline{\hat{e} \cdot \hat{e}'}|^2 = \frac{1}{2} \left(\frac{e^2}{Mc^2}\right)^2 (1 + \cos^2 \theta),$$

where the factor $\frac{1}{2} (1 + \cos^2 \theta)$ arises from the averaging over the spins and polarization directions of the incident and scattered photons. It is convenient to express the contributions to the total scattering amplitude in units of $\left(\frac{e^2}{Mc^2}\right)$. In this notation the Thomson scattering



MU-13147

Fig. 27. Differential cross section at 90° for the elastic scattering of gamma rays by protons.

amplitude becomes

$$S_{\text{Thomson}} = (\hat{e} \cdot \hat{e}').$$

The next scattering effect to be considered is that of the magnetic moment of the proton. Unlike the Thomson amplitude, the magnetic moment amplitude depends (linearly) on the primary photon energy. The magnetic moment of the proton is composed of two parts, the intrinsic (or Dirac) part and the anomalous part. For a rather obscure reason the scattering from these two parts of the proton total moment is not exactly the same, and is supposedly due to the quantum-mechanical treatment of the scattering from a current loop and a point (intrinsic) magnetic moment. If the anomalous magnetic moment is denoted by λ , in units of the intrinsic moment, $\left(\frac{e\hbar}{2Mc}\right)$, then the total magnetic moment is

$$\lambda + 1$$

The magnetic-moment scattering amplitude is given by several authors^{2, 3, 4} as

$$\begin{aligned} S_{\text{magnetic moment}} = & -i \alpha (2\lambda + 1) \hat{\sigma} \cdot (\hat{e} \times \hat{e}') \\ & + 2i (\lambda + 1)^2 \hat{\sigma} \cdot (\hat{e} \times \hat{k}) \times (\hat{e}' \times \hat{k}') \\ & + i \frac{\alpha}{2} (\lambda + 1) \{ \hat{\sigma} \cdot [\hat{k}(\hat{k} \times \hat{e}) + (\hat{k} \times \hat{e})\hat{k}] \cdot \hat{e}' \\ & + \hat{\sigma} \cdot [\hat{k}'(\hat{k}' \times \hat{e}') + (\hat{k}' \times \hat{e}')\hat{k}'] \cdot \hat{e}' \}, \end{aligned}$$

where $\alpha = \frac{k}{Mc} 2$ and $\hat{\sigma}$ is the unit spin vector of the proton; \hat{k} and \hat{k}' are unit vectors in the direction of the incident and scattered quanta. The physical significance of the first term is not clear; it represents electric dipole absorption and magnetic dipole emission or vice versa, and has no classical analogue. The second term is due to the magnetic dipole absorption in the action of the magnetic field of the incident photon on the magnetic moment causing rotational vibration and, because of this forced rotational vibration of the moment, it emits

magnetic dipole radiation. The last term is due to two effects: (a) magnetic quadrupole absorption associated with the translation vibration caused by the directional gradient of the incident magnetic field on the magnetic moment and the consequent electric dipole emission because of this vibration of the protons charge, and (b) electric dipole absorption associated with the translational vibration of the proton caused by the action of the electric field on the charge and the consequent magnetic quadrupole radiation because of this vibration of the magnetic moment. The magnetic-moment scattering amplitude is, of course, a spin-dependent interaction.

Mesonic polarization scattering is now considered. A simple description of this effect is that the incident photon induces in the charged meson cloud an electric and magnetic dipole in the direction of its electric and magnetic field vectors of the photon. Such induced dipole moments would not depend on the direction of the spin of the proton, i. e., the interaction would be spin-independent. As the polarization arises from a mesonic origin, and as it is known that the meson-production interaction is spin-dependent, then it would be expected that part of the polarization scattering is spin-dependent. The polarization amplitude, $S_{\text{polarization}}$, is then composed of a spin-dependent and a spin-independent part; and also in the discussion below, only the dipole polarization terms are considered. The classical spin-independent polarization is given by¹⁹

$$-A_E a^2 (\hat{e} \cdot \hat{e}') + A_M a^2 (\hat{e} \times \hat{k}) \cdot (\hat{e}' \times \hat{k}'),$$

where the first term is the electric dipole term and the second is the magnetic dipole term. The spin-dependent polarization amplitude is given by¹⁹

$$-B_E a^2 \hat{\sigma} \cdot (\hat{e} \times \hat{e}') + B_M a^2 \hat{\sigma} \cdot (\hat{e} \times \hat{k}) \times (\hat{e}' \times \hat{k}'),$$

where the first term is the electric dipole term and the second is the magnetic dipole term.

Finally, the resultant scattering amplitude is the sum of the above scattering contributions,

$$S = S_{\text{Thomson}} + S_{\text{magnetic moment}} + S_{\text{polarization}}.$$

The total scattering amplitude S is now grouped into electric and magnetic dipole terms, which are spin-dependent and spin-independent, and a quadrupole term due to the magnetic moment:

$$\begin{aligned} S = & a_E (\hat{e} \cdot \hat{e}') + i B_E \hat{\sigma} \cdot (\hat{e} \times \hat{e}') \\ & + a_M (\hat{e} \times \hat{k}) \cdot (\hat{e}' \times \hat{k}') + i B_M \hat{\sigma} \cdot (\hat{e} \times \hat{k}) \cdot (\hat{e}' \times \hat{k}') \\ & + \text{Quadrupole Term.} \end{aligned}$$

The coefficients in this expression follow from the amplitudes already described:

$$\begin{aligned} a_E &= 1 - A_E a^2, & B_E &= -(2\lambda + 1) - B_E a^2 \\ a_M &= A_M a^2, & B_M &= (\lambda + 1)^2 + B_M a^2. \end{aligned}$$

The quadrupole term is the last member of the magnetic moment scattering amplitude described in the magnetic moment section.

In the introduction, the formulas there follow from particular choices of the above coefficients. It should be pointed out that so far the effect of the proton recoil and the finite size of the proton have not been included. The inclusion of recoil appears mainly in the factor $(a'/a)^2$, which is due to the transformation of solid angle from the frame of the recoiling proton to the laboratory frame, and tends to lower the cross section. The finite size of the proton is accounted for, approximately, by a form factor f , as is done in the Stanford scattering experiments.²⁰ This correction lowers the cross section, but the effect is small (5%) for photon energies below 146 Mev.

With the inclusion of recoil and the finite size of the proton, the differential cross section becomes

$$\frac{d\sigma}{d\Omega} = \left(\frac{e^2}{Mc^2}\right)^2 f^2 \left(\frac{a'}{a}\right)^2 |S|^2.$$

Some special cases of the above formula, which were discussed in the introduction, are now treated. The Thomson proton cross section is obtained by throwing out all the scattering amplitudes except $A_E = 1$, and setting the form factor and recoil factor equal to one. If only the Thomson amplitude and the intrinsic magnetic-moment terms are kept, one obtains the proton Klein-Nishina formula if the recoil is accounted for relativistically (also with the form factor equal to one). If, furthermore, the anomalous magnetic moment is included, but not the polarization amplitude, then the Powell formula is obtained. The exact inclusion of recoil may be seen in the Powell formula, where not only the factor $(a'/a)^2$ appears but also the terms that vary as the square of the photon energy, a^2 , are actually given by aa' . This inclusion has the effect of lowering the magnetic moment term by a factor of $(1+a)^{-1}$. This reduces the resultant cross section by about 8% at 146 Mev. If the magnetic moment and the spin-dependent polarization scattering amplitude are neglected, the Rayleigh formula is obtained.

A simple special case of the differential cross section is obtained if it is assumed that the spin-dependent polarization amplitudes are zero. In this case the cross section is essentially the sum of the Rayleigh and Powell formulas. In this case, we have

$$\frac{d\sigma}{d\Omega} = \frac{1}{2} \left(\frac{e^2}{Mc^2} \right)^2 f^2 \left(\frac{a'}{a} \right)^2 \left\{ [(1 - A_E a^2)^2 + A_M^2 a^4] (1 + \cos^2 \theta) - 4A_M a^2 (1 - A_E a^2) \cos \theta + aa' (1 - \cos \theta)^2 + aa' f(\theta) \right\},$$

The term $f(\theta)$ is defined in the Introduction.

The neglect of the spin-dependent polarization amplitude is a serious omission, since such amplitudes are expected from the facts that mesons are produced through a spin-dependent interaction and that, though the square of these amplitudes may be small, the interference of these terms with the large magnetic moment amplitudes necessitates a considerable correction to the net scattering cross section.

As a first approximation, let us consider only the dipole scattering amplitudes of S:

$$S_{\text{dipole}} = a_E (\hat{e} \times \hat{e}') + i B_E \hat{\sigma} \cdot (\hat{e} \times \hat{e}') \\ + a_M (\hat{e} \times \hat{k}) \cdot (\hat{e}' \times \hat{k}') + i B_M \hat{\sigma} \cdot (\hat{e} \times \hat{k}) \times (\hat{e}' \times \hat{k}').$$

The differential cross section obtained with only these dipole terms is

$$\frac{d\sigma}{d\Omega} = \frac{1}{2} \left(\frac{e^2}{Mc^2} \right)^2 f^2 \left(\frac{a'}{a} \right)^2 [\{ |A_E|^2 + |A_M|^2 \} (1 + \cos^2 \theta) \\ + \{ |B_E|^2 + |B_M|^2 \} (3 - \cos^2 \theta) + (A_E A_M + B_E B_M) 4 \cos \theta].$$

The final step towards getting a cross section is to somehow evaluate the polarization amplitudes. Capps¹⁹ has obtained these values through the use of dispersion relations. By considering only the dipole amplitudes, and with the knowledge of the total photomeson cross section at essentially all energies, it is possible to arrive at the sign and magnitude of the quantities A_E , A_M , B_E , and B_M (the polarization amplitudes).

Since this experiment was done at 90° scattering angle and there is an additional simplicity in the theory for the scattering at this angle (the electric dipole and magnetic dipole amplitudes are 90° out of phase so they will not interfere), we will write down the differential cross section for 90° scattering angle. Scattering at 90° in the center-of-mass frame is not the same as scattering at 90° in the laboratory system; however, there is little difference at the energies of this experiment.

If the dipole cross section given above is expanded in terms of the various amplitudes attributable to the charge, magnetic moment, and polarization, one obtains the following formula for 90° scattering angle:

$$\begin{aligned} \frac{d\sigma}{d\Omega}(90^\circ) &= \frac{1}{2} \left(\frac{e^2}{Mc^2} \right)^2 f^2 \left(\frac{a'}{a} \right)^2 [1 + 44aa' + (A_E^2 \\ &+ A_M^2 + B_E^2 + B_M^2) a^4 - 2A_E a^2 \\ &+ 2 \{ B_E(2\lambda + 1) + B_M(\lambda + 1)^2 \} a^3]. \end{aligned}$$

Aside from the leading factors, which are the 90° Thomson cross section, the form factor, and the recoil factor, the contributions in the square brackets are, in order, (a) the Thomson scattering, (b) the magnetic moment scattering, (c) the polarization scattering, (d) the interference between the spin-independent polarization scattering and the Thomson scattering, (e) the interference between the spin-dependent polarization scattering and the magnetic moment scattering. This expression is correct except for a recoil correction of about 10%, and for the magnetic moment quadruple scattering interference with the polarization scattering (which has been neglected). This expression, using the polarization amplitudes given by Capps, is plotted in Fig. 27 along with the Powell and Klein-Nishina cross sections for 90° scattering angle. According to the Stanford experiments,²⁰ the form factor f^2 is given, approximately, by

$$f^2 = 1 - 0.05 \left(\frac{k}{132} \right)^2$$

The magnitude of the coefficient in this expression depends on the size of the proton, and the energy dependence is the low-energy approximation of the form factor.

C. Comparison With Other Experiments

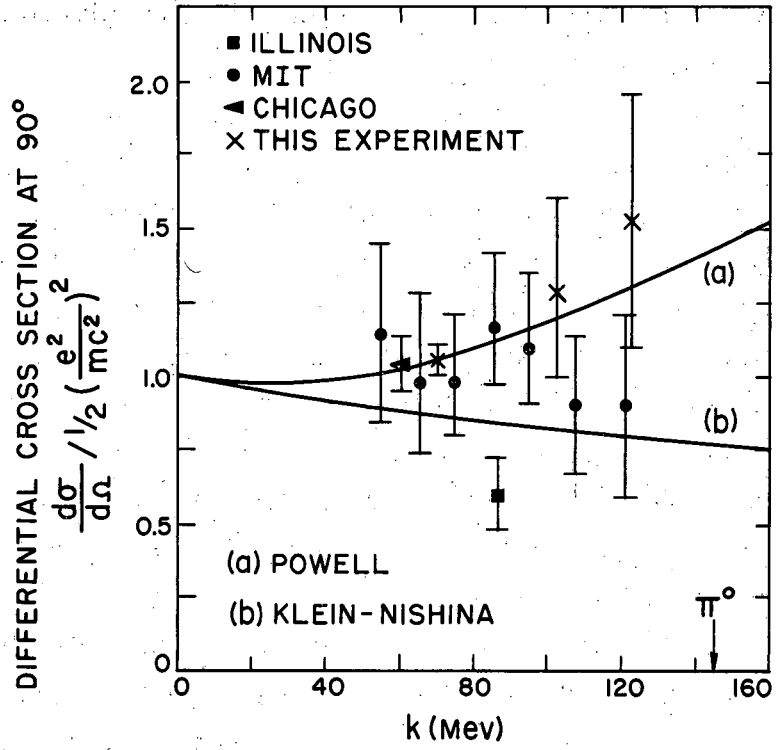
Results on elastic gamma-ray scattering by protons have only recently been obtained, owing to the experimental difficulties inherent in low-cross-section measurements. Available results are plotted in Fig. 28.

The first report on a cross-section value was by Mills at Illinois, where, in his experiment on photoproduction of neutral mesons, he obtained a value for the elastic scattering as a background point with the betatron set at 140 Mev.¹⁸ The point represents an average over the energy region from about 20 to 140 Mev. The statistics are not quoted, but from his activation data the errors seem to be about $\pm 20\%$.

Oxley and Telegdi at the University of Chicago measured the scattering at various angles averaged over the photon energy region 60 ± 35 Mev.²¹ Their 90° point agrees with the Powell cross section.

Pugh, Gomez, Firsch, and Janes at MIT. have carried out extensive experiments on nuclear scattering of gamma rays, including that by hydrogen, at various scattering angles and photon energies from 50 to 130 Mev.⁵ Their 90° hydrogen data are plotted in the figure, and tend to decrease at higher photon energies. Their two data points above 100 Mev lie below the cross section they expect theoretically and below the data points of this experiment.

The data points of this experiment are for 90° scattering angle and for photon energies ranging from 40 to 132 Mev. These results are shown in Fig. 28, and are normalized to the Powell cross section at 70 Mev. A comparison with the MIT data seems to indicate a disagreement, though the errors are rather large. The data points of this experiment suggest an increasing cross section as the photon energy approaches the meson threshold.



MU-13148

Fig. 28. Differential cross section at 90° for the elastic scattering of gamma rays by protons.

D. Summary

The differential cross section for the elastic scattering of gamma rays to 90° by protons has been measured for photon energies below the threshold for neutral meson production, in the region from 40 to 132 Mev.

The scattering is described by the Klein-Nishina formula for a particle of protonic mass that has been modified to include the additional scattering arising from (a) the large anomalous magnetic moment of the proton, and (b) the electric and magnetic polarizability of the mesonic structure of the proton.

The cross section is observed to increase with photon energy. The destructive interference between the Thomson and electric polarization amplitudes is out-weighted by the increasing scattering from the anomalous magnetic moment, and perhaps an increasing contribution from the interference between the polarization and the magnetic-moment amplitudes. For the wave lengths in this experiment, the effect of the finite size of the proton is of small importance.

ACKNOWLEDGMENTS

I wish to express my sincere thanks to Professor Burton J. Moyer for introducing me to the problem of the Proton Compton Effect and for his suggestions and encouragement during the course of this work. I am greatly indebted to Dr. Robert W. Kenney and Dr. John D. Anderson for their considerable assistance in carrying out the pair-spectrometer measurements of the synchrotron energy and for the loan of some counting equipment. I would like to thank Dr. Richard Capps for interesting discussions on the theoretical aspects of the experiment. Thanks are due Mr. Burns MacDonald for his help during the experiment and to Miss Lucy Lienesch who helped very much with the tedious film reading. I wish to express special gratitude to Mr. Rudin Johnson and the crew of the synchrotron for their excellent handling of the machine under the unusual operating conditions of this experiment.

This work was done under the auspices of the U. S. Atomic Energy Commission.

BIBLIOGRAPHY

1. J. L. Powell, Phys. Rev. 75, 32 (1949).
2. F. E. Low, Phys. Rev. 96, 1428 (1954).
3. M. Gell-Mann and M. L. Goldberger, Phys. Rev. 96, 1433 (1954).
4. A. Klein, Phys. Rev. 99, 998 (1955).
5. G. E. Pugh, R. Gomez, D. H. Frisch and G. S. Janes, Phys. Rev. (to be published).
6. R. G. Sachs and L. L. Foldy, Phys. Rev. 80, 824 (1950).
7. R. H. Huddleston, Compton Scattering on Nucleons, UCRL-2592, May 1954.
8. R. Capps and R. Sachs, Phys. Rev. 96, 540 (1954).
9. R. H. Capps and W. G. Holladay, Phys. Rev. 99, 931 (1955).
10. S. Minami, Progr. Theoret. Phys. (Japan) 9, 108 (1953).
11. Gell-Mann, Goldberger, and Thirring, Phys. Rev. 95, 1612 (1954).
12. J. D. Anderson, Production of Neutral Photopions as a Function of Atomic Weight, (Thesis), UCRL-3426, May 1956.
13. Powell, Hartsough, and Hill, Phys. Rev. 81, 213 (1951).
14. P. V. C. Hough, Phys. Rev. 74, 80 (1948).
15. L. I. Schiff, Phys. Rev. 83, 252 (1951).
16. L. I. Schiff, Phys. Rev. 70, 87 (1946).
17. W. Heitler, The Quantum Theory of Radiation, 3rd Ed. (Oxford, 1954).
18. F. E. Mills, Photo Production of Neutral Mesons from Hydrogen (Thesis), University of Illinois (1955).
19. R. H. Capps, UCRL-3572, Oct. 1956, and private communication.
20. R. W. McAllister and R. Hofstadter, Phys. Rev. 102, 851 (1956).
21. C. L. Oxley and V. L. Telegdi, Phys. Rev. 100, 440 (1955).